Mass-selected clusters on weakly interacting surfaces investigated with UPS

Dissertation
for obtaining the academic degree
Doctor rerum naturalium
(Dr. rer. nat.)

submitted by

Christoph Schröder

to Lehrstuhl Experimentelle Physik I
at the Fakultät Physik of the
Technische Universität Dortmund

July 2015

Printed: September 29, 2015 15:53h

Referee and Supervisor:	Prof. Dr. Heinz Hövel
Referee:	Prof. Dr. Dmitri Yakovlev
Chairperson:	Prof. Dr. Frithjof Anders
Scientific staff member:	Dr. Gerald Schmidt

Contents

Chapter 1

Introduction

Modern condensed matter and molecule physics cover ultrafast processes, extreme conditions, such as pressure or temperature, and smallest dimensions. [Feynman, 1960] imagined in a talk about new fields of physics, that a single bit of information will be stored in a particle of around 147 metal atoms. Furthermore he talked about single atom manipulation of samples and investigation of their properties. In the year 1959 these predictions sounded like fantasy, but nowadays a part of physics dealing with exactly these issues is cluster physics. A cluster is a small group of atoms and embodies the link between atom physics on the one side and solid state physics on the other. The properties of the clusters change heavily by adding or removing a single atom. In Ref. [Lim et al., 2010] the chemical properties of Au clusters depending on the size are investigated, showing that clusters can be used as a catalyst. An approach for a cluster as data storage device is presented in [Sessoli et al., 1993] using the cluster as a bistable magnetic unit.

During the last decade a tremendous amount of information about clusters was achieved, but for an industrial use many objectives have to be accomplished. A significant amount of properties of clusters observed in the gas phase can not be found for clusters deposited in or on materials due to interactions between the medium and the cluster. A way to deposit clusters on supporting materials, while retaining their properties has to be found.

The preparation and characterization of well-defined cluster-on-surface systems is the topic of this thesis. In order to investigate the electronic properties of clusters on surfaces ultraviolet photoelectron spectroscopy (UPS) was used, whereas low temperature scanning tunneling microscopy (STM) and low energy electron diffraction (LEED) was used for geometric surface characterization. A cluster beam facility provided a high flux mass-selected cluster

beam to deposit on samples located in a low temperature manipulator. The preparation and measurement was performed in situ to reduce the sample contamination.

For small metal clusters, with up to around 150 atoms per cluster, measured in the gas phase, quantized states in particular for highly symmetric clusters due to electronic and geometric filled shells in the cluster are described in the literature. The aim of this work is to investigate the influence of a weakly interacting surface with the clusters and to preserve those quantized states.

To work on these tasks, rare gas layers are adsorbed on flat surfaces of HOPG, Cu(111), Ag(111) and Au(111) to obtain a weak interaction between cluster and supporting material. In order to investigate the absolute energetic positions of clusters on rare gas layers, a model system with the resilient C_{60} molecule deposited on rare gas layers is studied.

Chapter 2 deals with the theoretical principles of clusters with the focus on their electronic structure. Also the experimental findings, from the literature, and present research challenges are presented. In chapter 3 the experimental methods (UPS, STM, LEED) and the corresponding experimental setup are described. An overview of the sample preparation processes is given in chapter 4. The results and discussion of C_{60} molecules and metal clusters on rare gas layers are presented in chapter 5.
A detailed description of the preparation of a thin Al_2O_3 layer on $Ni_3Al(111)$ surfaces as a cluster support for further experiments is given in chapter 6.

Chapter 2

Clusters

The following chapter contains information about the clusters used in this work and their electronic structure. A summary of previous measurements of clusters in the gas phase, which led to the experiments presented in chapter 5, is shown. Afterwards the experimental challenges for further measurements are described. More detailed information on clusters and their electronic structure are found in [Haberland et al., 1992].

Clusters are aggregates of equal atoms or molecules. In this thesis mainly copper and carbon atoms are used. Generally the size of clusters ranges from two or three to about 10^5 atoms and therefore represents the link between isolated atoms or molecules and bulk material. In this thesis the size range from 50 to 150 atoms is covered in which the properties of clusters differ significantly from molecules or crystals. For clusters without directed bonds the icosahedron shape is commonly favorable, which is shown for a Cu_{55} cluster in Fig. 2.1. The atoms form shells with 20 faces around one atom

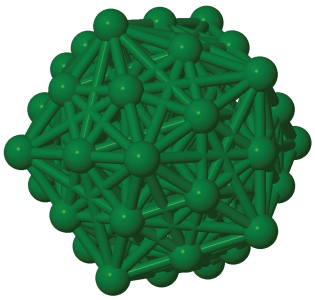

Figure 2.1: *An icosahedron with 55 copper atoms created with Jmol.*

in the middle. Electron diffraction is the method of choice to determine the geometrical structure of clusters in the gas phase. For example an icosahedral

shape was found for Ag_{55} clusters in Ref. [Schooss et al., 2005].
The electronic structure is heavily dependent on the size, shape and environment of the cluster. For the investigation of some topics for the influence of the environment it is useful to replace the metal clusters by C_{60} fullerenes in experiments. It is a carbon cluster with all atoms on the surface as shown in Fig. 2.2. The sp^2-hybridized carbon atoms form covalent bonds in contrast to the metallic bonds of the copper clusters. The C_{60} molecule is one of the most

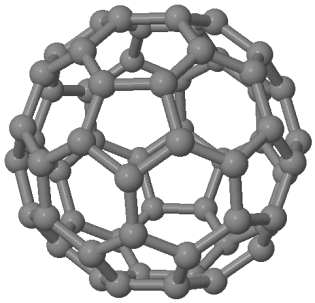

Figure 2.2: *A C_{60} molecule created with Jmol.*

resilient molecules [Lifshitz, 1993] and is therefore suited as a substitution of the copper clusters.

2.1 Electronic structure of clusters

A simple but accurate approach for the electronic structure of copper clusters is the spherical jellium model. The actually dot like positive charge of the atomic nuclei plus core electrons are assumed to be homogeneously distributed in the cluster, which leads to a potential for the delocalized electrons as shown in Fig. 2.3. The similarity to the Woods-Saxon potential, which is used to describe the forces in the nucleus, suggests the same classification of the states. This leads to closed electronic shells ($1s^2$ $1p^6$ $1d^{10}$ $2s^2$ $1f^{14}$ $2p^6$ $1g^{18}$ $2d^{10}$ $3s^2$ $1h^{22}$ ...) in the cluster for 2, 8, 18, 20, 34, 40, 58, 68, 70, 92 ... electrons in the valence band and therefore a higher stability of those clusters as it was observed for sodium clusters by [Knight et al., 1984]. When the cluster shape differs from a sphere the electron levels split up and the states are less degenerated. More information about the jellium model in regard to metal clusters can be found in [Brack, 1993].
For the photoemission process it is important to know that the energy needed to eject an electron from a metal cluster is approximately

$$E_{\mathrm{ej}} = \Phi + \left(z + \frac{1}{2} + c\right) \frac{e^2}{4\pi\epsilon(R+\delta)}, \tag{2.1}$$

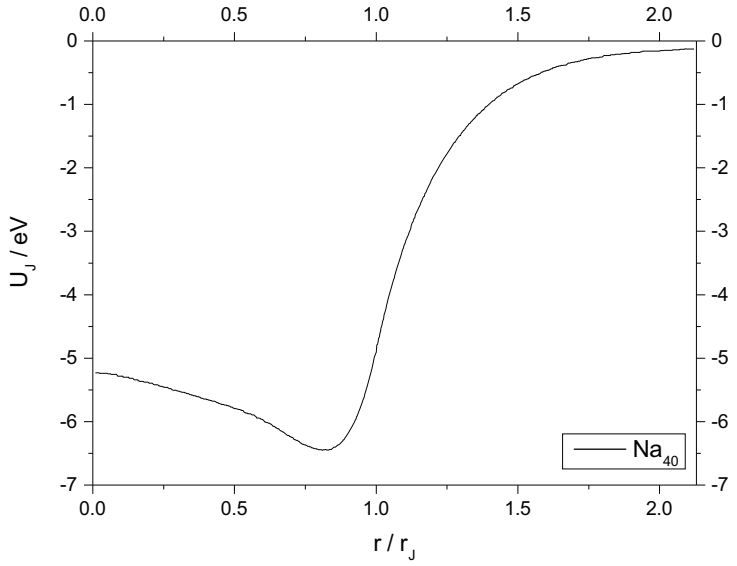

Figure 2.3: *The potential energy U_J of Na_{40} as a jellium sphere plotted against the radius in units of the jellium sphere radius r_J. The data was calculated by [Chou et al., 1984].*

with the work function Φ of the metal, the charge state z, the quantum correction c, the elementary charge e, the dielectric function ϵ of the surrounding material, the radius $R > 0.7\,\mathrm{nm}$ of the cluster and δ as a correction of the radius to include the fact that the probability of presence of the electrons reaches beyond the atoms of the cluster as shown in [Seidl et al., 1998]. This approximation is usable for the clusters presented in this work with a slight deviation for the smallest clusters. Depending on the charge of the cluster the energy is labeled as electron affinity E_{ea} for $z = -1$ and ionization potential E_{i} for $z = 0$.
An experimental verification of this approximation was done by [Hoffmann et al., 2002] as shown in Fig. 2.4. The onset of $\mathrm{Al}_{2000}^{-,n+}$ and $\mathrm{Al}_{32000}^{-,n+}$ clusters were studied, which are actually Fermi edge like due to the size of the clusters. Based on multiple ionization of the clusters during the photoemission measurement, the onset shifts by the charging energy

$$E_{\mathrm{C}} = \frac{e^2}{4\pi\epsilon(R+\delta)}, \tag{2.2}$$

of the clusters from ionization state n to $n+1$. This is in agreement with the energy needed to eject an electron in equation (2.1).

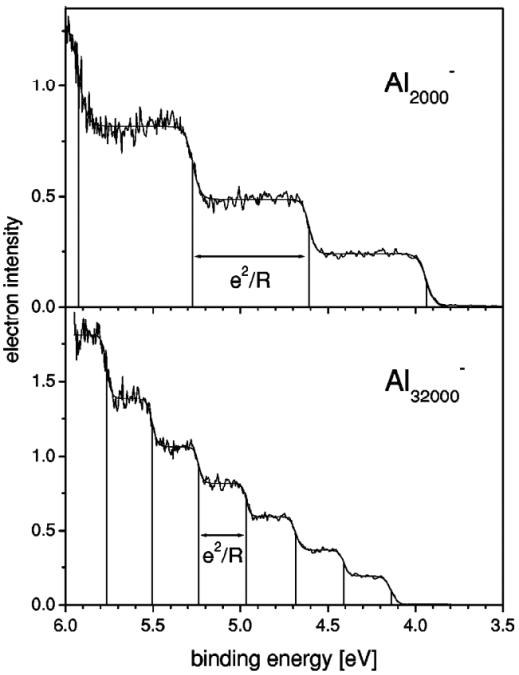

Figure 2.4: *UP spectra of $Al^{-,n+}_{2000}$ and $Al^{-,n+}_{32000}$ clusters measured with a photon energy of 6.42 eV from [Hoffmann et al., 2002]. Due to multiple ionization the cluster spectra show several onsets shifted by the charging energy from equation (2.2).*

2.2 Experimental findings

By regarding the theoretical model of the previous section it can be predicted that spherical clusters have highly degenerated quantized states. In order to obtain experimental evidence UPS measurements of clusters in the gas phase are shown. UPS is a technique to gain information about the electronic structure of the valence band region of a cluster or a surface and is explained in section 3.1.1. The clusters were measured in the gas phase with no contact to a surface to avoid the influence of the environment on the electronic structure and the deformation of the particle due to the deposition.
In Fig. 2.5 the electronic structure of copper clusters is shown, investigated with UPS by [Cheshnovsky et al., 1990; Taylor et al., 1992] and [Häkkinen et al., 2004; Kostko, 2007]. The displayed region is the s-p-band of the clusters, which is a term from bulk physics and labels the region between the d-band and the Fermi level. A discussion of the deviations between spectra for equal or similar sizes is done in chapter 5. It is striking that the electronic states highly vary with the cluster size. Cu_{55} and Cu_{147} have closed geometric icosahedral shells and therefore a nearly spherical shape. The neutral Cu_{92} has a closed electronic shell, with the assumption of a spherical shaped cluster. This prediction can be made, because in Ref. [Kostko et al., 2007] it was shown that the Na_{92} has a icosahedral shape with ten faces covered by a slightly rotated layer, which is called a subshell closing and results in an approximately spherical cluster as well. Sodium and copper show similarities in the electronic configuration by having the outermost s-shell filled with one electron. That makes the comparison between the cluster properties reasonable. The similarities between sodium, copper and silver are discussed in Ref. [Kostko, 2007]. The UP spectra of sodium, copper and silver cluster were scaled, taking into consideration that the clusters are made of materials with different effective mass and Fermi energy. This leads to a good agreement between the spectra, which are shown for the example of 55 atoms in Fig 2.6. It can be noted that the icosahedral symmetry of the clusters is the reason for highly degenerated and quantized states as it was explained with the jellium model in the previous section.
In Fig. 2.7 from [Häkkinen et al., 2004] the UP spectra, which is in principle the density of states, of copper and silver cluster anions in the gas phase with 53, 55, 57 and 58 atoms are shown. Only the clusters with 55 atoms show highly degenerated states due to their icosahedral symmetry. Cu_{57} clusters show a splitting of the degenerated states, due to the two additional atoms attached to the Cu_{55} core. Additionally the electronic shells of the cluster anions with 57 atoms are filled, therefore the spectra of the cluster with 58 atoms show a new feature corresponding to a new electronic shell.

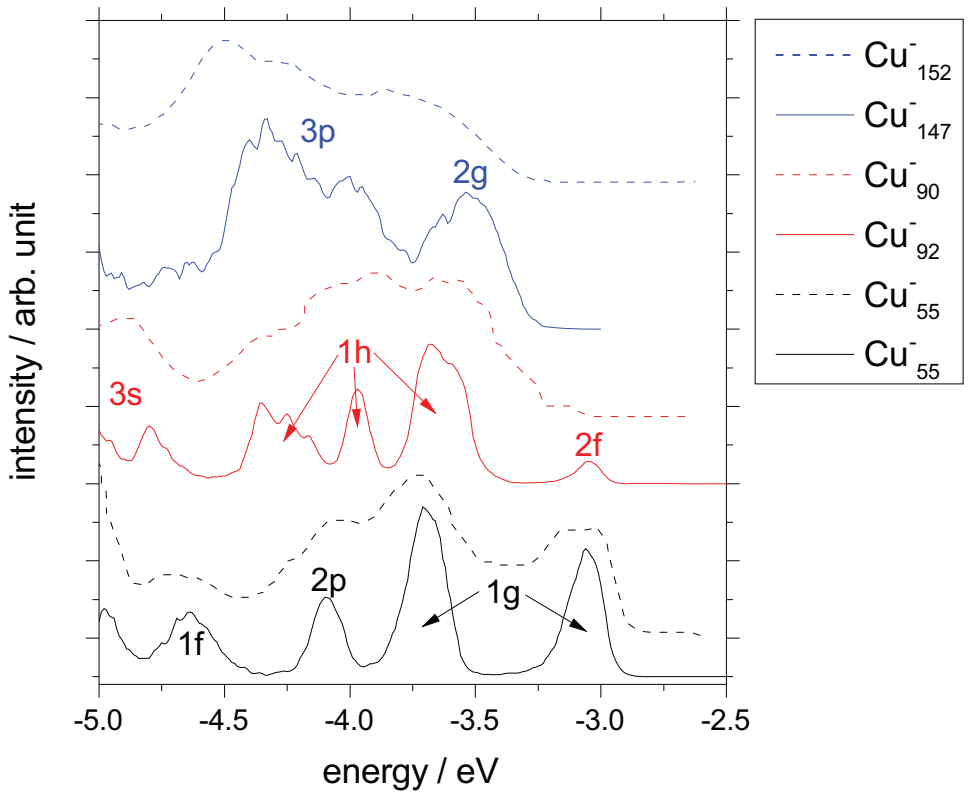

Figure 2.5: *Photoelectron spectra of negatively charged copper clusters displaying the electronic states in the clusters. The dashed lines are from [Cheshnovsky et al., 1990; Taylor et al., 1992] measured with 7.9 eV photon energy and 0.15 eV energy resolution digitalized from the publication and the solid lines are from [Häkkinen et al., 2004; Kostko, 2007] measured with 6.42 eV photon energy and 0.03 eV energy resolution provided by courtesy of von Issendorff. The spectra are normalized and shifted vertically for a better comparability. The labels of the electronic states are consistent with the jellium model. 0 eV labels the vacuum energy, which is the reference energy for clusters or molecules in the gas phase.*

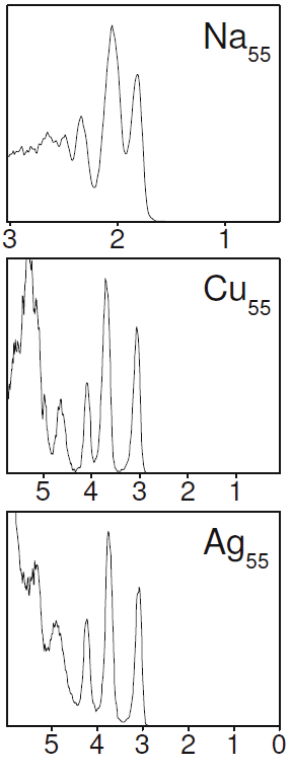

Figure 2.6: *Comparison between UP spectra of sodium, copper and silver cluster in the gas phase with 55 atoms from Ref. [Kostko, 2007]. The spectra were scaled, taking into consideration that the clusters are made of different materials.*

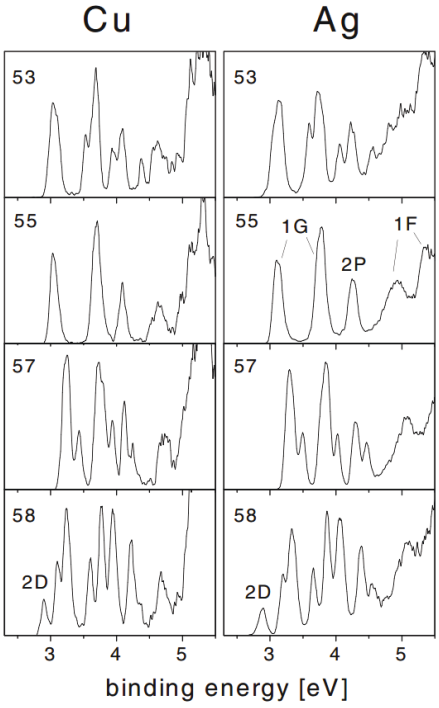

Figure 2.7: *UP spectra of copper and silver cluster anions in the gas phase, which represents the density of states of the clusters. For 55 atoms highly degenerated states occur, due to the high symmetry of the icosahedral cluster shape. The clusters with 58 atoms show, in comparison to the clusters with 57 atoms, an additional occupied shell, because of the filled electronic shells. The spectra are from [Häkkinen et al., 2004].*

2.3 Experimental challenges

There are several uses of small particles with quantized states such as computing or catalysis. But for most of the applications the clusters have to be deposited on a material or in a matrix. The experimental challenge, especially of this work, is to investigate if it is possible to maintain the quantized states and to understand the influence of the surroundings on the cluster.
Deposited clusters have to fulfill several prerequisites in order to show the quantized states as shown in Fig. 2.5. The clusters have to be mass-selected, because a broad mass distribution leads to a superposition of several different electronic structures. A contamination of the clusters would have a similar effect and also lead to unreliable data. The deposition energy has to be low enough to prevent the cluster from deforming or fragmenting. A cold substrate furthermore avoids the diffusion and possibly an alloying of the cluster with the substrate. For scanning tunneling spectroscopy low cluster coverages are sufficient, but up to now no precise interpretation of the electronic structure extracted from ST spectra of clusters was published. In Ref. [DeMenech et al., 2007] calculations to simulate ST spectra of a cluster were done. The simulations show a strong dependence of the spectra on the shape of the tip. Even for very sharp tips a measurement would be very selective, which leads to a low number of detectable states at a certain position on the cluster. An experimentally very challenging recording of several spectra of different positions on a single cluster would be needed to characterize the electronic structure of the cluster.
For a more straightforward interpretation an averaging method like UPS is more suitable. The disadvantage is that UPS relies on high coverages and therefore on high cluster fluxes, because a prolongation of the deposition time is not an option due to sample contamination.

In [Siekmann et al., 1993] an early photoemission measurement of Pb_{500} clusters deposited on SiO_2/Si is presented. No reliable signal of the s-p-band region of the lead cluster could be obtained. The reason for that can be a low mass resolution and deposition energies between 1 eV and 2 eV per atom. A more recent X-ray photoelectron spectroscopy measurement by [Peters et al., 2013] is about small deposited mass-selected copper clusters. The clusters were soft-landed (< 1 eV per atom) on a p-doped SiO_2/Si(100) with a mass resolution of $m/\Delta m \approx 100$. The spectra show no signal in the s-p-band region especially due to the high photon energy (200 eV).
In Ref. [Wortmann et al., 2010], using the same setup as in this work, UPS measurements of deposited mass-selected silver clusters are shown. The Ag_{55} clusters were deposited with a kinetic energy of 0.02 eV per atom at 50 K on

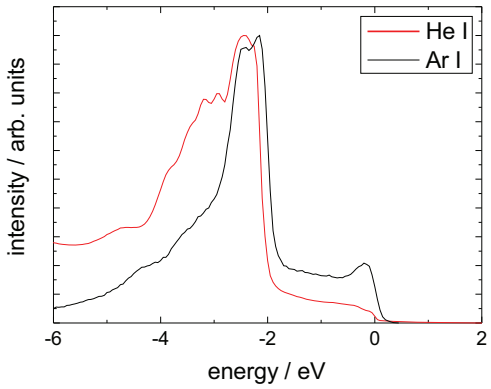

Figure 2.8: *Two measurement of a polycrystalline copper crystal are shown. The gas discharge lamp operated with argon shows more sensitivity to the s-p-band region.*

HOPG and UP spectra were measured with a photon energy of 21.2 eV. The signal in the s-p-band region is very low in contrast to the prominent d-band peak, which could be attributed to a significant influence of the cluster surface interaction and higher photon energy compared to the gas phase experiment shown in Fig. 2.5.
Up to now no signal in the s-p-band region of clusters comparable to the measurements in the gas phase was published. The approach in this work is to lower the cluster surface interaction by using adsorbed rare gas layers. With the use of a photon energy of 11.62 eV the sensitivity to the signal of the s-p-band region increases. To demonstrate that effect an UPS measurement of polycrystalline copper is shown in Fig. 2.8. The spectra are normalized on the d-band to compare the s-p-band of the signal. The s-p-band region measured with a gas discharge lamp operated with argon has more intensity and shows more features then the other spectra measured with helium.
Another approach is to prepare a system with immobile clusters without low temperatures by using oxidized surfaces with electronically active sites as described in chapter 6.

Chapter 3

Experimental access

This chapter deals with the experimental methods used to obtain information about the electronic structures of clusters described in chapter 2. The main technique is ultraviolet photoelectron spectroscopy (UPS), whereas scanning tunneling microscopy (STM) and low energy electron diffraction (LEED) are mentioned additionally. The specification of each apparatus is described in detail. In addition the experimental setup including the cluster production and mass selection in the cluster beam facility will be described. The sample preparation and investigation instruments in the analysis and preparation chambers are presented last.

3.1 The basis for measurement

The method used here to investigate the electronic structure of the clusters is UPS. STM and LEED only play a secondary role and are used to determine the surface quality.

3.1.1 Ultraviolet photoelectron spectroscopy (UPS)

The photoemission process can be described with a semiclassical three-step model from [Berglund and Spicer, 1964b,a]. A quantum mechanical approach from [Feibelman and Eastman, 1974] shows that for a narrow distribution of the photoelectron momentum Fermi's golden rule results in the three-step process and therefore justifies the use of this model.
In the first step a photon with the energy $\hbar\omega$ hits the sample and penetrates the surface. The photon excites an electron in the bulk, which causes the annihilation of the photon. The electron is excited from an initial state to an unoccupied final state but remains at its geometric position throughout this

process.
The second step represents the transition of the electron to the surface. The dominant scattering process during the transport is caused by electron electron interaction.
In the third step the electron is transferred from the bulk to the vacuum. The electron requires a minimal kinetic energy perpendicular to the surface to overcome the barrier defined by the work function Φ of the surface. Slower electrons are reflected back into the bulk.
The kinetic energy of the ejected electrons

$$E_{\mathrm{kin}} = \hbar\omega - E_{\mathrm{B}} - \Phi$$

can be analyzed to obtain information about the binding energy E_{B} of the electrons and therefore the density of states of the sample. For clusters the work function is replaced with E_{ej} from equation (2.1) on page 4

$$E_{\mathrm{kin}} = \hbar\omega - E_{\mathrm{B}} - \Phi - \left(z + \frac{1}{2} + c\right) \frac{e^2}{4\pi\epsilon(R+\delta)}.$$

The reference energy for UP spectra in surface science experiments is commonly the Fermi energy E_{F} and in gas phase experiments the vacuum energy E_{vac}.

A schematic of the setup used for UPS in this work is shown in Fig. 3.1. The ultraviolet photons are provided by a gas discharge lamp operated with argon. A lithium fluoride (LiF) window was installed to separate the gas

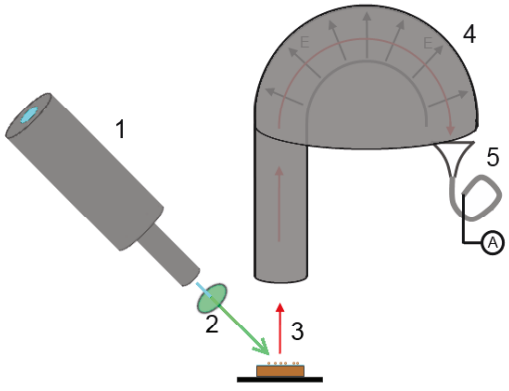

Figure 3.1: *The gas discharge lamp (1) operated with argon emits light, which is monochromatized (2) by a LiF window to 11.62 eV. The kinetic energy of the electrons ejected from the sample (3) are analyzed by a hemispherical energy analyzer (4) and measured with five channel electron multiplier (5).*

discharge lamp from the rest of the vacuum chamber to prevent the argon from adsorbing on the cold sample. More information about the installation and construction can be found in Ref. [Miroslawski, 2010]. LiF has a temperature dependent UV transmission as described in [Budke and Donath, 2008; Suga et al., 2010], which allows to monochromatize the argon light with a window temperature of 72 °C. The photon energy of the remaining Ar I line is 11.62 eV and the wavelength 106.7 nm.
UPS is a very surface sensitive method, because the electron escape depth in this low energy regime is just a few monolayers of the sample. The kinetic energy of the electrons is investigated with a hemispherical energy analyzer and measured with five electron multipliers simultaneously. The entrance orifice is set to 2 mm and the exit slit to 6 mm for an optimized flux with an energy resolution of 0.15 eV.
Angle resolved photoelectron spectra can display the entire band structure of a sample but provides no additional information for samples investigated in this work, because the clusters are oriented randomly on the surface. All measurements presented in this work are done in normal emission with an acceptance angle of $\pm 8°$, which results in a measurement spot of 1.21 mm in diameter. If at high photon flux and low conductivity of the sample static charging effects occur, it is indicated by a time depending shift of the spectra to lower energies.

3.1.2 Scanning tunneling microscopy (STM)

The scanning tunneling microscope is a tool to image the surface geometry of a conducting sample on the atomic scale. The underlying effect of this method is the quantum tunneling process, which occurs at thin potential barriers. An electron has a certain probability to tunnel through this barrier although it is classically impossible. This effect has an exponential distance dependence, which leads to a distance sensitivity in the tunneling current of approximately one order of magnitude per 1 Å [Gimzewski and Möller, 1987]. Scanning a surface with a sharp tip and a constant tunneling current it is possible to obtain the topography of the sample.
[Tersoff and Hamann, 1985] presented a simple theory for the tunneling process with the approximations of low temperatures, small voltages and a spherically symmetric s-wave function in the tip. It was found that the tunneling current is proportional to the local density of states of the surface. The image obtained by the STM is a convolution of the local density of states of the tip and sample weighted by the tunneling probability.
A schematic STM setup is shown in Fig 3.2. The sharp tip, commonly consisting of tungsten, is approached to the conducting sample with the use

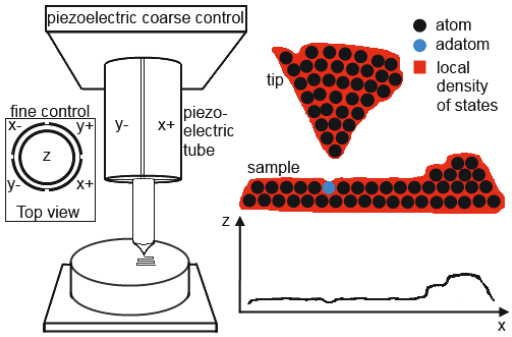

Figure 3.2: *The left part of the figure shows a sketch of the setup used for STM. The tip is moved by piezoelectric elements to approach and scan the sample. In the right a schematic of the tip on the surface is shown. The local density of states and therefore the STM image shows a dip at the position of the adatom even though all atoms are evenly distributed on the flat surface.*

of a piezoelectric coarse control. The fine control of the tip, used to scan the sample, is done by a piezoelectric tube. A voltage applied between tip and sample causes a tunneling current, which is in the magnitude of 1 nA at 0.5 nm distance. The tip is chemically etched at atmospheric pressure, afterwards it is cleaned and sharpened in UHV by heating and sputtering processes [Albrektsen et al., 1994]. It has to be said that it is not possible to investigate the clusters on 60 monolayers xenon with STM, because the rare gas layer is not sufficiently conductive.

3.1.3 Low energy electron diffraction (LEED)

In this work low energy electron diffraction (LEED) is used to investigate the long range order of the first few monolayers of a surface. Figure 3.3 shows a schematic of a LEED setup. An electron beam with a narrow velocity distribution and an adjustable kinetic energy of 20 eV to 500 eV is directed on a sample parallel to the surface normal. The low penetration depth of these low energetic electrons is the reason for the high surface sensitivity. Only the elastically backscattered electrons reach the spherical fluorescence screen located around the sample. In the case of long range ordered surface symmetries the scattered electrons interfere and form a pattern on the screen, which is an image of the reciprocal lattice of the surface. This can be used for a qualitative evaluation of the atomic arrangement and distances. A more detailed description about LEED can be found in Ref. [Lüth, 1993].

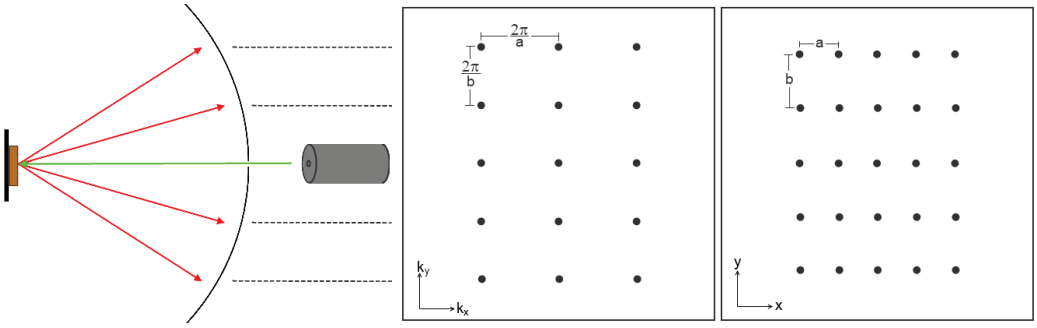

Figure 3.3: *An electron gun provides electrons with an adjustable kinetic energy of 20 eV to 500 eV, which are scattered on the surface of a crystal. The elastically backscattered electrons fall on the fluorescence screen leading to the image in the reciprocal space (k_x,k_y) and the corresponding image in the real space (x,y).*

3.2 Experimental Setup

The experimental setup can be divided into two parts. In the preparation and analysis chamber, sample preparation and measurements are performed. The cluster beam facility provides a semi-continuous positively charged mass-selected cluster beam.

3.2.1 Cluster beam facility

In this section a short overview of the cluster beam facility is given. A detailed description can be found in Ref. [Duffe, 2009]. The cluster beam facility itself can be divided into three sections as shown in Fig. 3.4. All chambers are pumped with a turbomolecular pump separately.

Cluster source The clusters are produced in a magnetron sputter gas aggregation source. A target of the cluster material is sputtered with argon ions to eject atoms. The atoms accumulate by collisions with argon and helium in an aggregation region. The helium and argon flux in addition to the length and outlet aperture of the aggregation region can be varied to change the mass distribution of the produced clusters. Due to the formation process the clusters are mainly singly charged. This cluster source was invented by [Haberland et al., 1994].

Cryochamber The charged clusters are transported by electrostatic lenses through a skimmer into the cryochamber, where the residual gas, except of

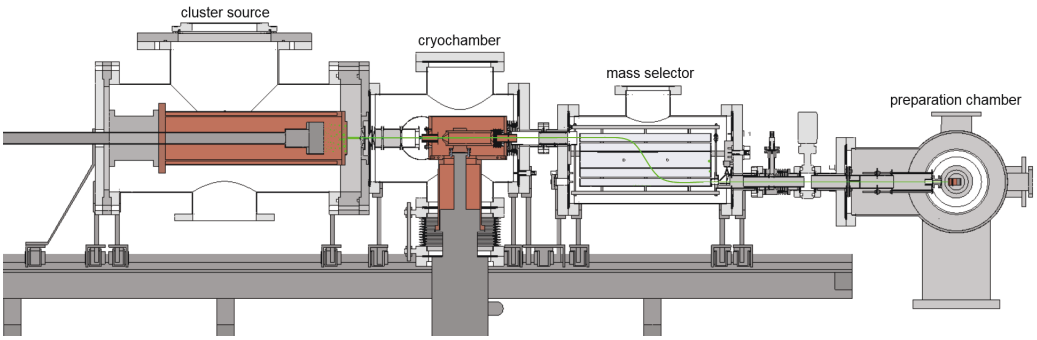

Figure 3.4: *The setup of the cluster beam facility. Clusters are produced in a magnetron sputter gas aggregation source. A cluster beam is formed and focused in the cryochamber and mass-selected by a time-of-flight semi-continuous mass selector. The last electrostatic lenses focus the cluster beam on a sample in the preparation chamber.*

helium, is frozen out at the cold surface of the cryopump.

Mass selector The cluster beam is focused by further electrostatic lenses, which lead the clusters into the mass selector. It is a semi-continuous time of flight mass selector as presented in [von Issendorff and Palmer, 1999]. The equally charged clusters are accelerated perpendicular to their direction of motion by an electric field. The variation in the mass of the clusters lead to different velocities and therefore a splitting of the cluster beam by mass. Applying a reverse electric field to stop the perpendicular motion results in a displacement and therefore a mass selection of the beam. The period of time between those two electrical pulses is related to the selected cluster mass. Only the chosen part of the split cluster beam passes the exit aperture of the mass selector, which leads to further electrostatic lenses. The mass-selected cluster beam is focused to 1 mm in diameter with a high flux for short deposition durations. A mass spectrum of copper clusters is shown in Fig. 3.5. The mass resolution $\frac{m}{\Delta m} = 39$ is calculated by averaging the quotients of the cluster masses and the full width at half maximum of the Gaussian fits. This is not the best mass resolution achievable with this setup but a good compromise between short adjusting times and good resolution. A linear fit of the peak positions is used to extrapolate the cluster masses of clusters with 40 or more atoms. The mass selector is the only part of the cluster beam facility, which has a direct connection to the preparation chamber during measurements, therefore it has to be baked to reach base pressures below 10^{-8} mbar.

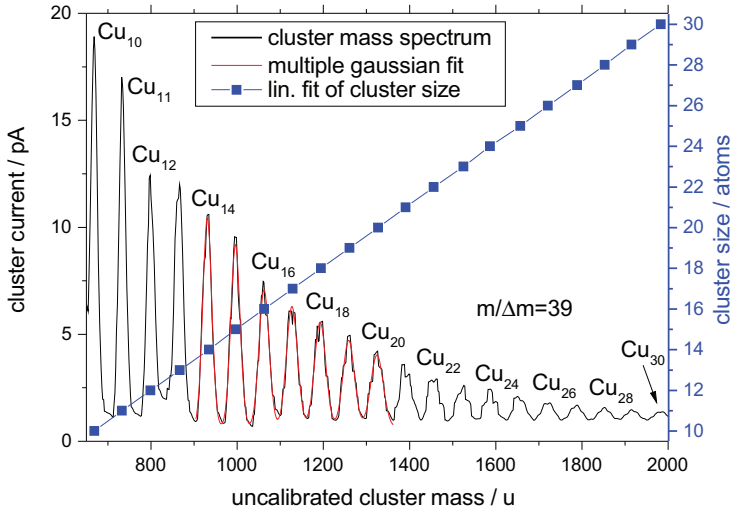

Figure 3.5: *A mass spectrum of copper clusters with 10 to 30 atoms. The mass resolution is* $\frac{m}{\Delta m} = 39$ *calculated by Gaussian fits. A linear fit of the exact peak positions is used to extrapolate higher cluster masses.*

3.2.2 Preparation and analysis chamber

The preparation and analysis chamber are two parts separated by a valve. The base pressure in these chambers is below 10^{-10} mbar. Both chambers are pumped with a titan sublimation pump and ion getter pump, additionally the analysis chamber can be pumped with a turbomolecular pump during sample cleaning or preparation processes.

Manipulator The manipulator is a device to hold a sample during cleaning and preparation processes. Samples in the manipulator can also be transferred between the analysis and preparation chamber along the z-axis. Translations in the direction of the x- and y-axis, also rotations around the z-axis can be performed to reach each preparation or analyzing device. There are three different sample holders attached to the manipulator. The low temperature sample holder can cool the sample down to 10 K. The temperature is not measured directly at the sample surface, however the deviation between sample temperature and measured temperature is below 5 K. For STM tip preparations a sample holder for field emission, sputtering and heating procedures is installed. The heatable sample holder can achieve sample temperatures above 900 K.

Measuring instruments In the analysis chamber the only device, besides a storage for 6 samples, is a low temperature STM, with the operating temperatures of 5 K (liquid helium), 77 K (liquid nitrogen) and 300 K (room temperature), which is described in section 3.1.2. For STM measurements the sample has to be vibration damped, therefore the measurements are not performed in the manipulator, in contrast to UPS or LEED measurements, but in the STM sample holder. Sample transfer into the STM is realized using a small auxiliary manipulator.
To perform LEED measurements, as discussed in section 3.1.3, the cluster beam facility has to be removed from the preparation chamber. This is the reason for the low number of LEED measurements in this work.
The gas discharge lamp and electron analyzer, needed for UPS measurements explained in section 3.1.1, are permanently attached to the preparation chamber.

Sample preparation instruments A sputter gun is installed in the preparation chamber in order to remove thin oxide films and impurities from the surface of a sample or an STM tip by argon ion impact.
To obtain lower pressures during heating processes and higher maximum temperatures than the heatable sample holder of the manipulator can achieve, a heating station was build and installed during this work. Sample temperatures of 1150 K and pressures below 10^{-9} mbar can be reached simultaneously. The maximum sample temperature is above 1400 K. More details about the heating station can be found in section 6.2.1.
For xenon and argon there is a gas inlet at the preparation chamber, krypton was inserted using a valve of the cluster beam facility.

Vacuum lock To transfer samples into the UHV without breaking the vacuum and prevent resulting bake out processes a vacuum lock is attached to the preparation chamber.

Chapter 4

Sample preparation

In this chapter each preparation step for clusters on rare gas layers will be described in detail. It starts with a short paragraph about cleaning the substrates which serve for rare gas adsorption. The parameters of the rare gas adsorption will be presented and additionally LEED and UPS measurements are shown to support the chosen process. The last part deals with the cluster and C_{60} deposition procedure.

4.1 Rare gas layers adsorption

In order to create a defined environment for the clusters the adsorbed rare gas layers should be flat and well ordered.

The first step is to produce a flat and clean underlying substrate. HOPG, Cu(111), Ag(111) and Au(111) were used because of their flat surfaces and different work functions. Detailed information on the substrates can be found e.g. in Ref. [Dederichs et al., 1983].
HOPG was tape cleaved to get a clean and flat surface before the transfer into UHV. The graphite was heated to 600 °C for one hour to evaporate the remaining adsorbates.
The preparation of the three noble metal samples was done by a three step process. It started with heating the sample to increase the diffusion of impurities or defects to the surface. Then the samples were sputtered by argon ions with $E = 1000\,eV$ and $I = 2.5\,\mu A$ for one hour to remove the top layers of the surface. A following heating step repaired the roughened surface. This process was repeated until the surface state appears as a narrow peak in the UPS signal, which is an indication for a clean, flat and well ordered surface [Hüfner, 2003].

There are three different rare gas configurations used for the presented results in chapter 5. For all experiments a xenon layer was adsorbed on the surface. The rare gas layer has to be thick enough to suppress the cluster substrate interaction and thin enough to avoid a static charging effect of the sample during UPS measurements. A third criteria is that electrons ejected from the substrate beneath the xenon layer should not be able to pass through the layer to avoid signal in a region where we expect the cluster signal. It was found in previous experiments that for xenon a suitable amount is 60 monolayers [Irawan et al., 2006]. For argon and krypton no suitable thickness was found, because static charging effects occur before the suppression of the substrate signal was sufficient. Therefore ten monolayers of argon or krypton were adsorbed on top of the xenon layer to obtain a sample which fulfills the three criteria but also to investigate three different cluster surface interactions.
In Fig. 4.1 the phase diagram of xenon on Ag(111) is shown. The two

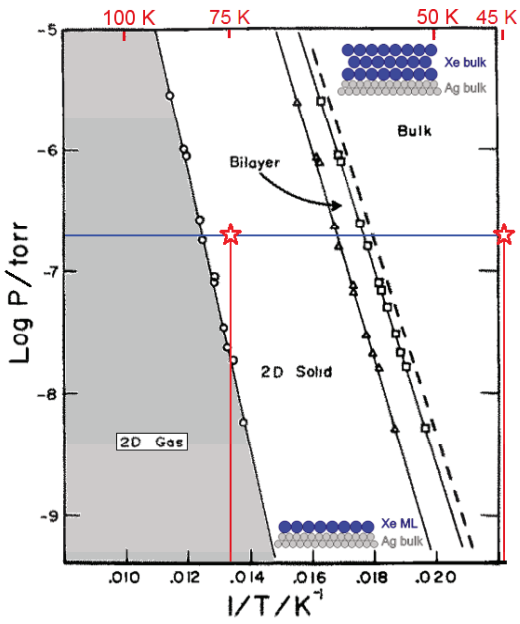

Figure 4.1: *Phase diagram of xenon adsorption on Ag(111). The stars mark the positions where one and 60 monolayers are adsorbed. This diagram is a modified version from [Unguris et al., 1979].*

positions marked by a star were used to adsorb either one monolayer of xenon or bulk xenon on the surface. The first monolayer was adsorbed at 75 K and $2.61 \cdot 10^{-7}$ mbar to obtain exactly one monolayer (ML) of xenon. With a high adsorption duration and the relatively high temperature the xenon

atoms form a well ordered layer. When the first monolayer was adsorbed the temperature can be lowered to 45 K with $2.61 \cdot 10^{-7}$ mbar for 19 minutes to adsorb 60 monolayers. The estimation of the adsorption duration was done by observing the position of the prominent $5p_{1/2}$ state of xenon with UPS and is explained in more detail in [Irawan et al., 2006]. After the adsorption the xenon pressure and sample temperature were lowered simultaneously.
At this point there are three different options. Most experiments were done with only 60 monolayers of xenon and no other rare gas. The other two options are with 10 monolayers of krypton or 10 monolayers of argon on top of the 60 monolayers xenon to decrease the cluster surface interaction even further. The adsorption process of krypton and argon is similar to the adsorption process of xenon but with different temperatures. In the case of argon the first monolayer was adsorbed at 25 K and $1.01{\cdot}10^{-7}$ mbar for 120 s and the following nine monolayers at 12 K and $1.01{\cdot}10^{-7}$ mbar for 400 s. For krypton, there was no indication of a layer by layer growth measurable by UPS with 11.62 eV photon energy. That is the reason for a short adsorption duration of the first monolayer at 20 K and $5.15{\cdot}10^{-8}$ mbar and the remaining nine monolayers at 12 K and $5.15{\cdot}10^{-8}$ mbar for 400 s. A summary of all adsorption parameters is listed in Table 4.1.

	first monolayer			remaining monolayers		
	p / mbar	T / K	t / s	p / mbar	T / K	t / s
60 ML xenon	$2.61{\cdot}10^{-7}$	75	120	$2.61{\cdot}10^{-7}$	45	1140
10 ML krypton*	$5.15{\cdot}10^{-8}$	20	20	$5.15{\cdot}10^{-8}$	12	400
10 ML argon*	$1.01{\cdot}10^{-7}$	25	120	$1.01{\cdot}10^{-7}$	12	400

Table 4.1: *The parameters used for all rare gas adsorption processes in the presented experiments. All pressures are measured with an ionization gauge calibrated to N_2 but corrected (multiplied) by a scale factor of 0.775 for Ar, 0.515 for Kr and 0.348 for Xe. *on 60 ML xenon*

To demonstrate the importance of this two step adsorption process LEED measurements of xenon adsorption on Cu(111) are shown in Fig. 4.2. Adsorbing 60 monolayers xenon at 13 K no reflex can be found in the LEED measurement whereas the two step adsorption process presented above provides an ordered xenon layer indicated by the only slightly blurred reflexes.
The work function of a substrate is an indication of the surface roughness, as it was shown for copper in Ref. [Li and Li, 2005]. The UP spectra in Fig. 4.3 show the onset of the xenon spectra, which represents a difference in the work function of the layers. Both spectra are referenced to the Fermi energy at 0 eV. To calculate the work function of the xenon the photon energy has to

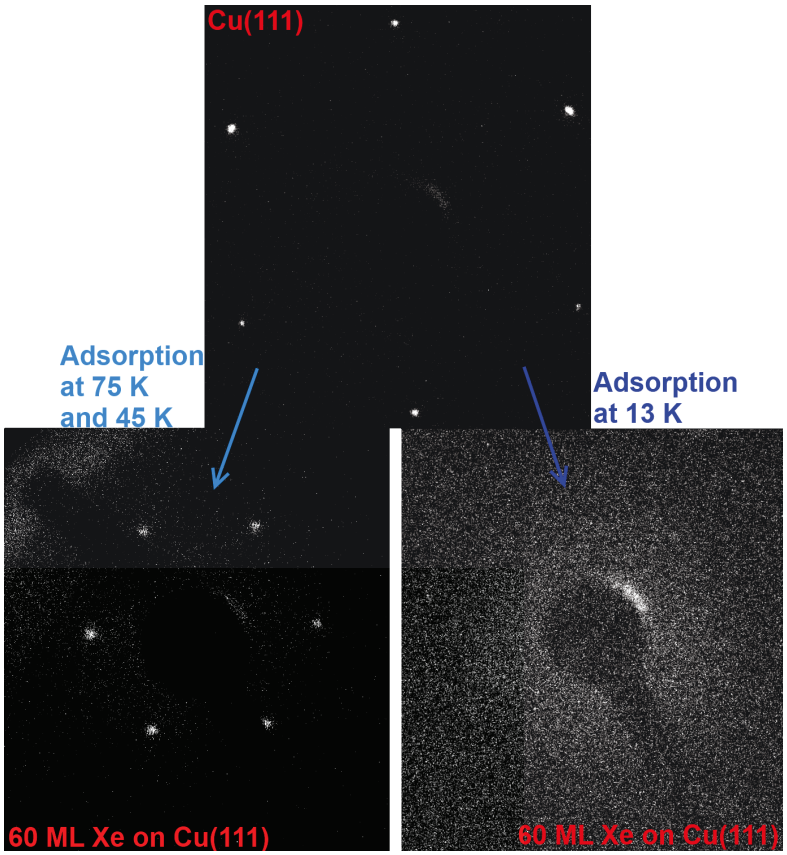

Figure 4.2: *At the top a LEED measurement of a clean Cu(111) surface is shown. In the bottom left diffractogram 60 monolayers were adsorbed in two steps, as described in the text, is displayed. Adsorbing the rare gas at 13 K leads to the measurement in the bottom right. The background light comes from a ionization gauge. The two step process provides an ordered xenon layer on top of the sample in contrast to the one step adsorption process where no long range order can be seen in the LEED measurement, even though the ionization gauge was turned off and the contrast was optimized. Measurements were done with an electron energy of 90 eV and a sample temperature of 13 K. The images are depicted in black and white with an increased contrast.*

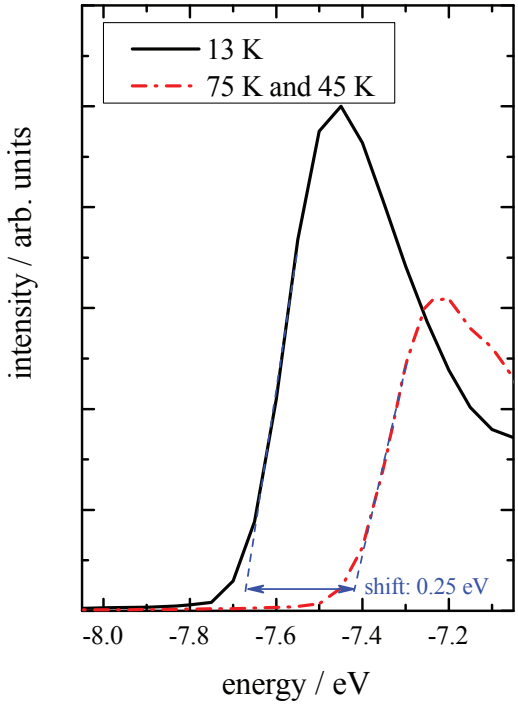

Figure 4.3: *UP spectra showing the onset of the Xe $5p_{1/2}$ signal using two different adsorption procedures. The difference in the onset is equal to the difference in the work function, which is an indication for the roughness of the surface. The two step adsorption process has a higher work function and therefore a smoother surface.*

be subtracted by the width of a spectra. This means the work function of the two step adsorption xenon layer is 0.25 eV higher than for the single step process. This corroborates the formation of a flat surface for the two step process and therefore a more suitable environment for the clusters.

4.2 Cluster and C_{60} deposition

The cluster beam facility from section 3.2.1 was used to produce a mass-selected semi continuous metal cluster beam. The last aperture of the ion optics allows to create cluster deposition spots with 1 mm in diameter. This supplies enough room for at least nine deposition spots on a 1 cm^2 sample with different cluster sizes or coverages for a good comparability. The kinetic energy of the charged clusters is reduced by an electric field to less than 10 eV per cluster. In Fig. 4.4 the cluster current is plotted as a function of the deceleration voltage applied in the faraday cup. The voltage was set to the

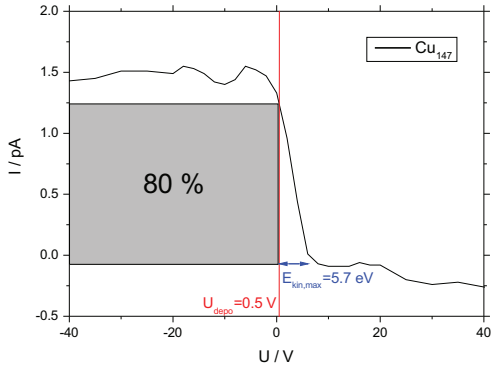

Figure 4.4: *Cluster current measured with a Faraday cup plotted versus the applied voltage. The deposition voltage of 0.5 V is applied to the sample with a cluster current of 80 % for a soft-landing of the clusters.*

marked value to have a high current and a low kinetic energy of the clusters as described in the supplementary materials of [Grönhagen et al., 2012].
For the following experiments it was necessary that the clusters are isolated from each other. Therefore, in most measurements, a coverage of about 10000 clusters per μm^2 was chosen for the most probable distance of 4.5 nm calculated as described in [Knorr et al., 2002]. For a Cu_{147} cluster the coverage of the surface can be calculated to less than 2 % of a cluster monolayer. The radius can be estimated by assuming the cluster has the same density as bulk copper. As long as the coverage is lower than 10 % of a cluster monolayers the majority of the randomly deposited clusters are isolated [Sieben, 2007].

A low coverage has the disadvantage of a low UPS signal, which complicates the localization of the deposition spots. That is the reason why the first deposition spot on the sample has a high coverage and cluster mass, showing a prominent UPS signal. Once the spot with the high coverage was found, UPS measurements of all other spots, where clusters will be deposited, were taken to obtain the background signal of every single spot. The clusters were subsequently deposited on these positions and measured afterwards with UPS.
The temperature during deposition is equal to the temperature mentioned for each specific UPS measurement.

A C_{60} evaporator was used to deposit C_{60} molecules on rare gas films with a deposition spot of about 1 cm in diameter. In order to determine the deposition rate a quartz crystal oscillator was used for the calibration and further adjustments were done with STM images. For all experiments presented the deposition time was 19 s, which yields a coverage of 6.25 % cluster monolayers. The deposition energy can be estimated by the thermal energy during the evaporation process to less then 0.1 eV per molecule. The thermal radiation of the C_{60} crucible could lead to an evaporation of the rare gas layers during the deposition process. Therefore the sample cooling helium flow was increased and the temperature did not rise above 15 K.

Chapter 5

Results and Discussion

In this chapter clusters and molecules deposited on rare gas layers measured with UPS are presented and discussed. The first section is about C_{60} on rare gas as a model system for a better understanding of the more complex system of clusters on rare gas layers, which are compared to UPS measurements of clusters in the gas phase layers in the second section. Several of the copper and silver cluster spectra shown in this chapter were measured in cooperation with [Miroslawski, 2013], but additional measurements were needed for a full interpretation of the data.
The work functions of the used substrates are listed in table 5.1.

Materials	Φ [eV]
HOPG	4.5[a]
Cu(111)	4.94[b]
Ag(111)	4.74[b]
Au(111)	5.31[b]

Table 5.1: *The work function Φ of the surfaces used.* [a] *[Pivetta, 2003; Pivetta et al., 2005]* [b] *[Goldmann, 2003]*

5.1 C_{60} on rare gas layers

The sample preparation and C_{60} deposition is explained in chapter 4. UPS, additionally to the used setup, is demonstrated in section 3.1.1.
C_{60} molecules were deposited on three different rare gas layer systems adsorbed on three different metal surfaces. This leads to the following nine sample variations

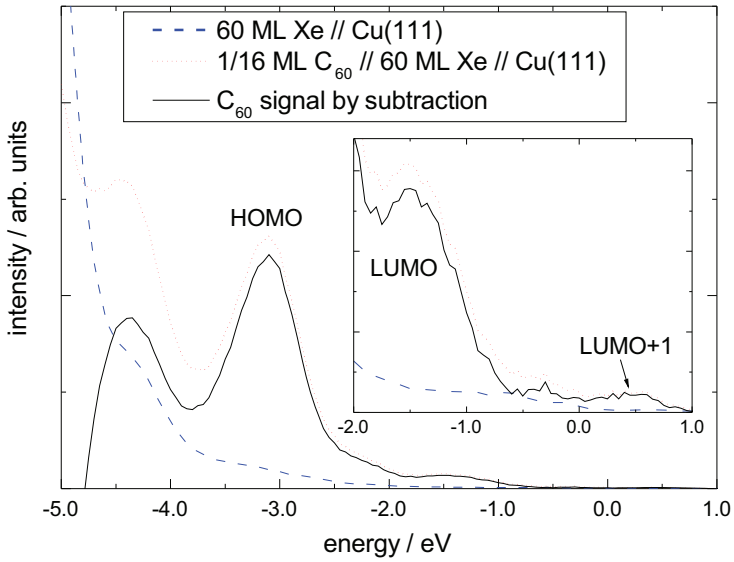

Figure 5.1: *Two UP spectra of the same spot before and after C_{60} deposition on 60 ML xenon on Cu(111). The C_{60} signal is obtained by subtracting these two spectra. At -3.1 eV the highest occupied molecular orbital (HOMO) is visible. The inset magnifies the lowest unoccupied molecular orbital (LUMO) and the LUMO+1. All spectra are normalized on the HOMO peak hight.*

- C_{60} on 60 ML xenon on Cu(111)
- C_{60} on 60 ML xenon on Ag(111)
- C_{60} on 60 ML xenon on Au(111)
- C_{60} on 10 ML krypton on 60 ML xenon on Cu(111)
- C_{60} on 10 ML krypton on 60 ML xenon on Ag(111)
- C_{60} on 10 ML krypton on 60 ML xenon on Au(111)
- C_{60} on 10 ML argon on 60 ML xenon on Cu(111)
- C_{60} on 10 ML argon on 60 ML xenon on Ag(111)
- C_{60} on 10 ML argon on 60 ML xenon on Au(111)

The sample temperature during deposition and measurement was 10 K. For each sample UP spectra before and after C_{60} deposition were recorded as shown for C_{60} on 60 ML xenon on Cu(111) in Fig. 5.1. The integration

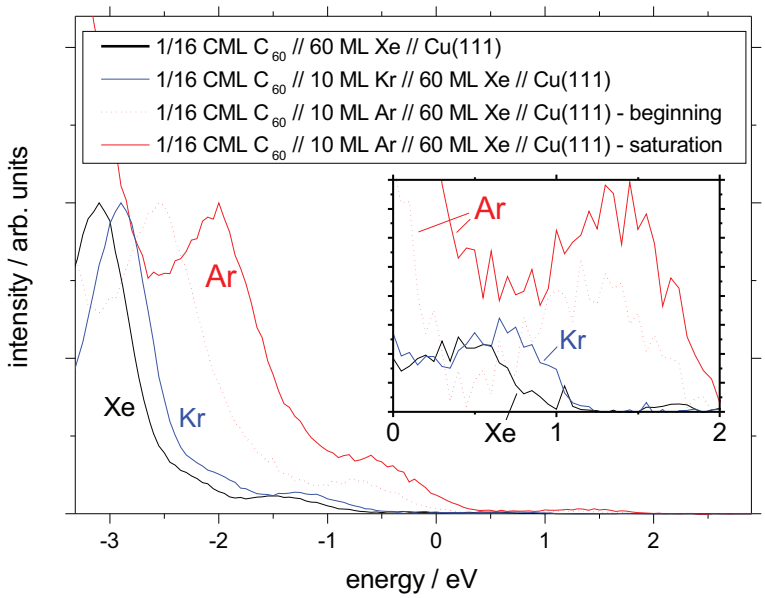

Figure 5.2: *Subtracted C_{60} signal on three different rare gas layers adsorbed on Cu(111). The signal to noise ratio is much worse for argon, because averaging the spectra was not possible due to a shift over time between the single spectra. Therefore the first and last spectrum is shown to display the shift. An overview of all measurements can be found in Fig. 5.4 on page 33.*

time of a each data point was 1 s and the step width 0.05 eV, which leads to approximately 230 s including all delays for one series. Five spectra were recorded before and 16 to 20 after the C_{60} deposition. The background signal was smoothed with the Savitzky-Golay method over 10 points and polynomial order of 2 to compensate the lower statistics. When the change of the spectra in the different series was just caused by statistical fluctuations, the spectra were added and normalized on the measurement duration. In order to obtain the C_{60} signal the spectra after deposition were subtracted by the smoothed background signal. The prominent peak at -3.1 eV is the highest occupied molecular orbital (HOMO). Also the lowest unoccupied molecular orbital (LUMO) and LUMO+1 can be seen in the inset in Fig. 5.1. All spectra of the C_{60} molecule shown in this section were normalized on the HOMO peak height.

For krypton and xenon the extraction of the C_{60} signal was done as described above. In the case of argon a time dependent shift of the spectra to higher energies occurred as shown in Fig 5.2. For a qualitative analysis the HOMO signals were fitted by Gaussian functions to obtain the positions, which are plotted against the measurement time in Fig 5.3. There was no defined point

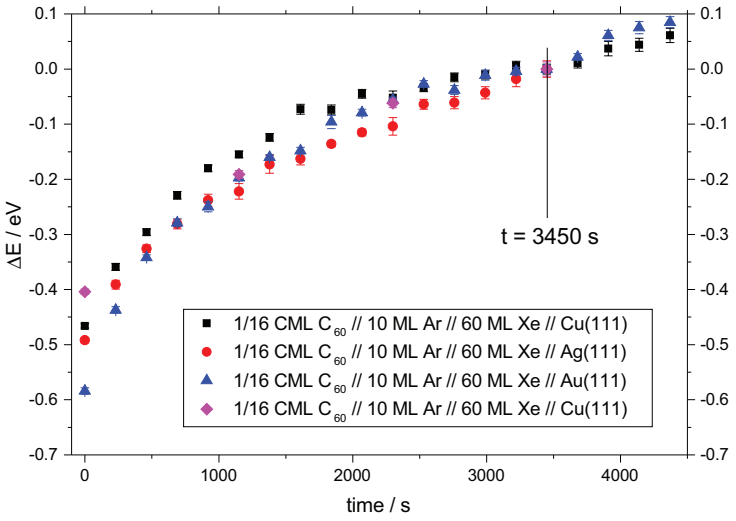

Figure 5.3: *The saturation curve of C_{60} on argon adsorbed on three different metal substrates with the error from the Gaussian fit. A measurement of a newly prepared sample with a fifth light exposure on Cu(111) is shown to verify that the charge transfer is independent of the photoemission process.*

in time when the clusters were deposited, therefore the energy shift was referenced for all four curves to the time 3450 s, which is the last point on Ag(111). In the beginning the change of the energy shift is comparably high and reaches a saturation region after 2000 s to 3000 s. Also an independent measurement of a newly prepared sample on Cu(111) is shown. The light exposure was lowered to 20 % of the time by measuring only every fifth series and transferring the sample out of the UV light beam for the rest of the time. There is no significant change in the saturation curve and therefore the independence of the charging process on argon by the light exposure can be verified.

The C_{60} signal was extracted as described before, which leads to the spectra shown in Fig. 5.2 or 5.4. By comparing the shift of the HOMO with the shift of the LUMO and LUMO+1 on argon in Fig. 5.4, it is noticeable that the shifts of the LUMO and LUMO+1 are smaller. This effect can at least partially be explained by calculated Kohn-Sham orbital energies of C_{60} and C_{60}^- from [Green et al., 1996] shown in Fig. 5.5. In the case of a neutral C_{60} molecule the states, especially the HOMO, are highly degenerated. For a C_{60}^- anion a splitting of these states leads to less degeneration and a smaller gap between the HOMO and the LUMO, which is similar for the LUMO+1 state. This leads to a decrease of the gap between HOMO and LUMO or LUMO+1

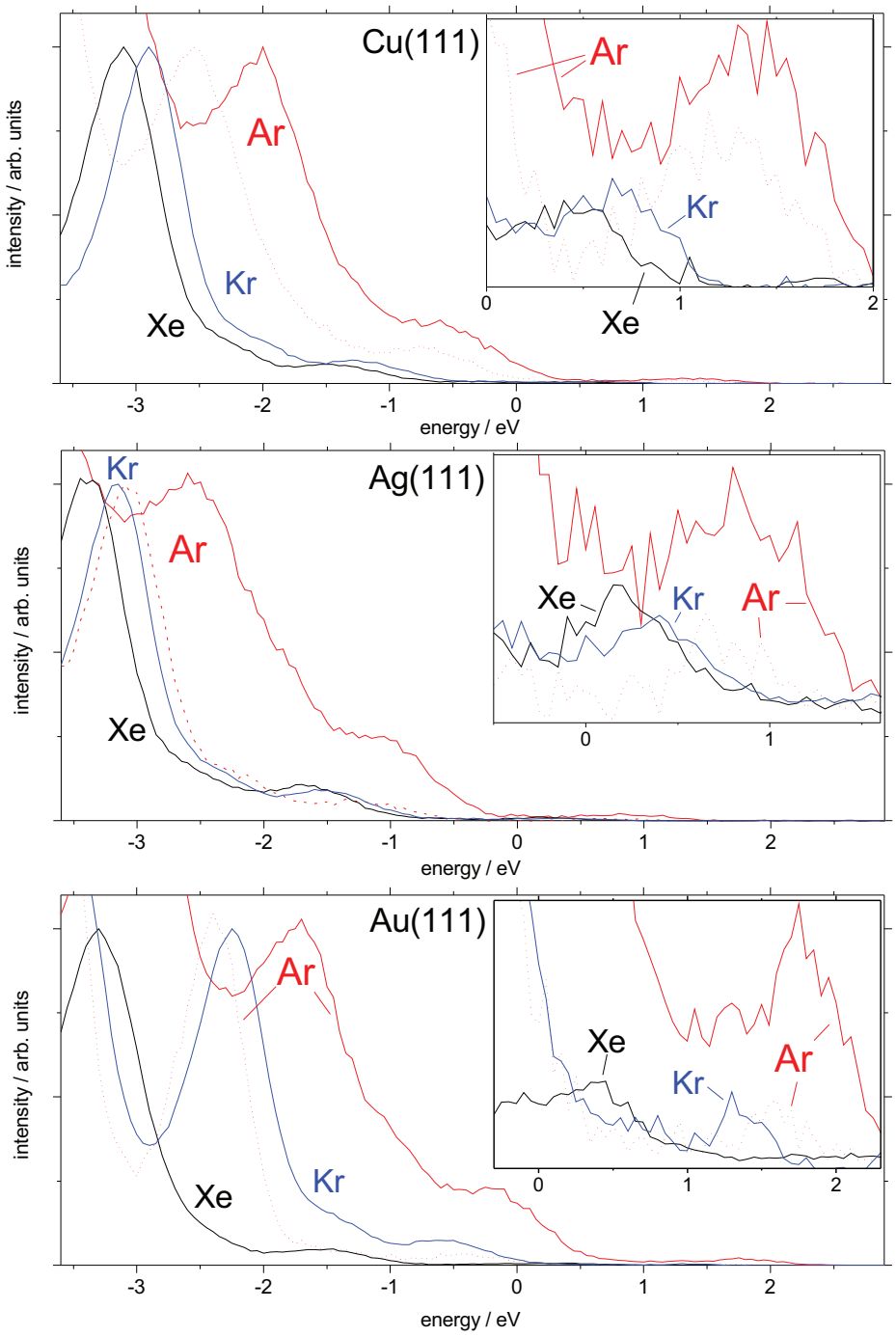

Figure 5.4: *An overview of all C_{60} measurements showing the HOMO, LUMO and LUMO+1 signals.*

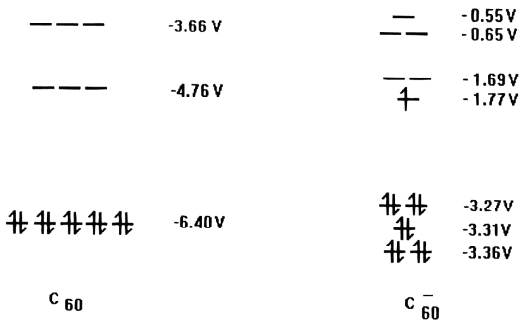

Figure 5.5: *Calculated energy pattern with density functional theory from [Green et al., 1996], showing a decrease of the HOMO-LUMO gap due to a splitting of the highly degenerated states.*

respectively, which explains at least partially the differences in the shifts.
The position of the HOMO of these measurements, is shown in Fig. 5.6. For argon just the saturated measurements were used. The values were subtracted by the work functions of the substrate respectively for a better comparability. From [Zimmerman et al., 1991] the energy of the HOMO, which equals the ionization potential of the molecule, was given as 7.61 eV and is marked with a star symbol. The data shows a linear dependence between the HOMO peak position and the electron affinity of the rare gas layer. The dashed line indicates that the slope is actually -1, that means the shift of the HOMO as compared to a free C_{60} molecule is equal to the electron affinity of the rare gas layer. A significant deviation can be found for xenon on Au(111). Deviations from the concept of *quasi-free* clusters on rare gas layers were already observed for metal island growth on xenon adsorbed on Au(111) in Ref. [Irawan et al., 2006] and lead to the assumption of a specific behavior of this configuration. An explanation for the shift of the HOMO with the electron affinity of the rare gas is a partial charging effect of the C_{60} molecules. This can be observed in the inset of Fig. 5.2, where the LUMO+1 state of argon has less intensity before saturation than in saturation. The filling of the unoccupied state, while the intensity of lower energy states remains the same even without normalization of the HOMO peak height, indicates a charge transfer to the molecule. Additionally the time dependent shift in Fig 5.3 of the HOMO peak of C_{60} on argon corresponds quantitatively to the electron affinity of argon (-0.4 eV). In contrast the saturation for the partial charging on Kr and Xe is supposed to be so fast that it was finished already before the first UP spectra.
For the quantitative interpretation of the following cluster spectra, it has to be taken into consideration that the energetic position of the spectra of particles

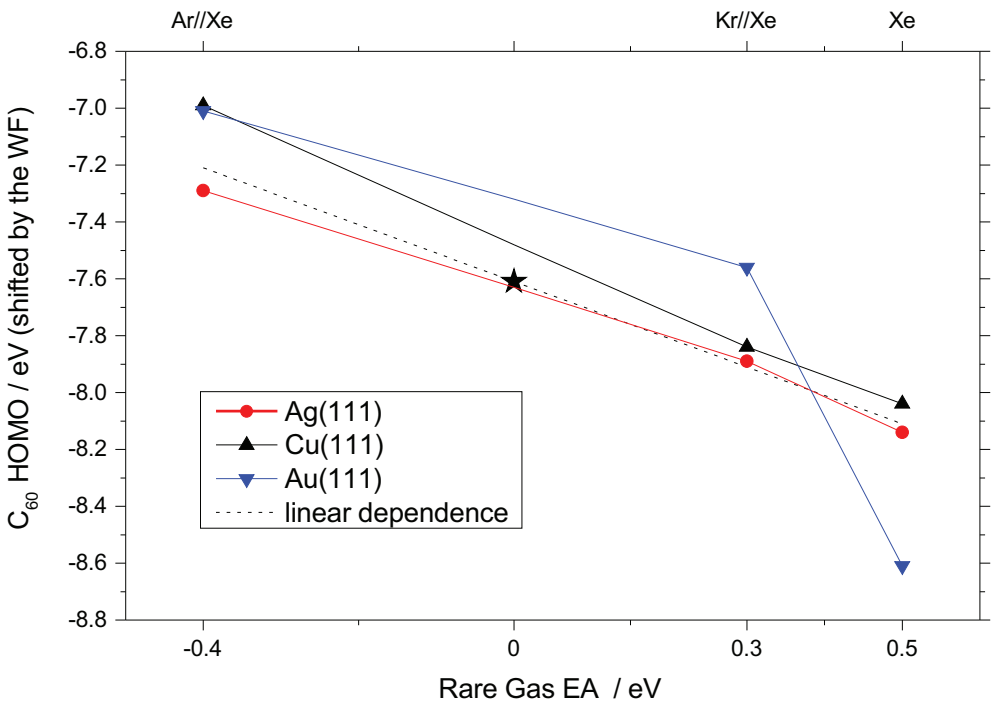

Figure 5.6: *An overview of the energetic position of the HOMO peak of C_{60} molecules deposited on 9 different samples is shown. The star symbol marks the HOMO peak position of C_{60} in the gas phase of 7.61 eV from [Zimmerman et al., 1991]. A dashed line with the slope of -1 indicates that the shift of the HOMO peak is equal to the electron affinity of the rare gas layer. The electron affinity values are from [Klein and Venables, 1977].*

on surfaces is shifted by the electron affinity of its supporting material.
For a better understanding of the charging process and the reason why it occurs, further investigations of the time dependent energy shift for argon should use exactly defined deposition times and prolonged measurements to obtain a flat plateau in the end of the saturation. A theoretical approach to obtain more information about this mechanism might give the answer why the time scales of the charging processes are so different for Ar versus Kr and Xe. The electron loss of the C_{60} molecule is amplified by the photoemission process, which could be a reason for a faster charge transfer on krypton and xenon. However no influence of the photoemission process on the charging transfer on argon was measured.
For xenon and krypton the LUMO and LUMO+1 state are partially occupied even though the molecules should be partially positively charged. Generally, however the energetic position, at least of the LUMO, below E_F of the substrate may allow some occupation. In that notion the positive charge is an additional partial charge.

Summary It was found that the ionization energy of C_{60} molecules, deposited on various rare gas layers, changes with the electron affinity of its surrounding medium. In the case of argon the corresponding partial charging process of the C_{60} molecules could be observed over one hour. This eventually causes the shift of the ionization energy by the electron affinity.

5.2 Clusters deposited on rare gas layers

A detailed description of the preparation, deposition and measurement procedure of metal clusters deposited on rare gas layers can be found in chapter 4. The photoemission process and the used setup is presented in section 3.1.1. UP spectra before and after deposition of the clusters were subtracted to separate the cluster signal from the background spectra. In order to compare the cluster signal from the deposition experiment to the gas phase experiment the spectra have to be shifted according to their reference energy, charge state and electron affinity of the surrounding material of the cluster. In Fig. 5.7 the shift for Cu_{147}^- in the gas phase for a comparison with Cu_{147} on xenon is shown to explain the routine done for all following measurements. As already mentioned in chapter 3 the reference energy of surface science experiments is commonly the Fermi energy E_F and the work function is the energy difference between the Fermi level and the vacuum energy E_{vac}. An approximation of the energy needed to eject an electron from a metal cluster isolated from the substrate is shown in equation (2.1) on page 4. The onset of the spectra of

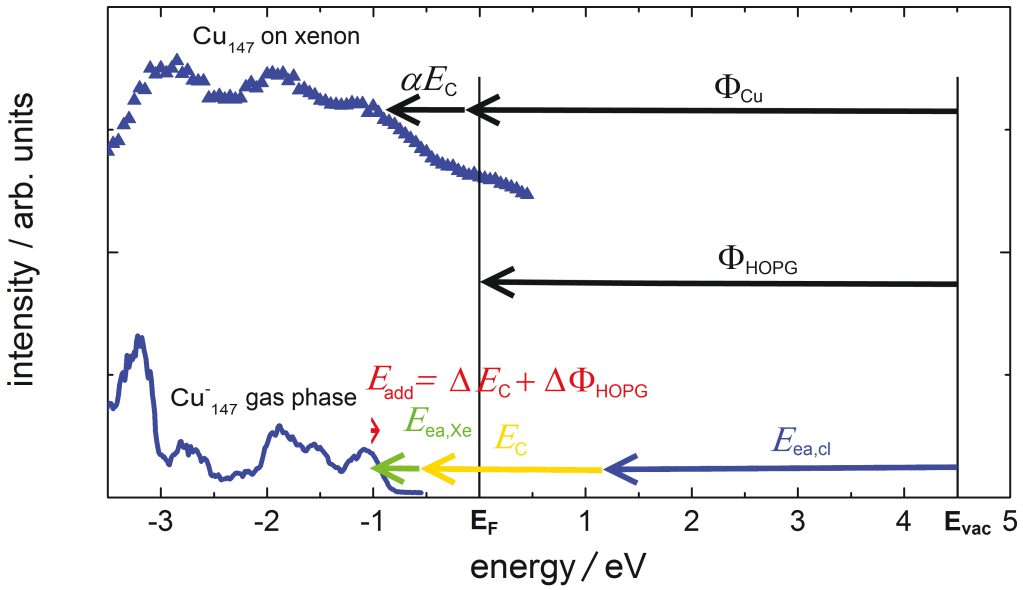

Figure 5.7: *A visualization of the shifts to compare clusters deposited on rare gas layers with clusters in the gas phase. The reference energy in surface science experiments is commonly the Fermi energy E_F, which is the work function of the substrate (HOPG) below the vacuum energy E_{vac}. The energy needed to eject an electron from a neutral Cu_{147} clusters on xenon is $\alpha E_C + \Phi_{Cu}$ as shown in equation (2.1) on page 4 with $\alpha = \frac{1}{2} + c$ and the charging energy E_C from equation (2.2) on page 5. To eject an electron from a cluster anion in the gas phase the electron affinity of the cluster $E_{ea,cl}$ is needed. For a comparison of neutral clusters and cluster anions the clusters have to be shifted by the charging energy E_C. As discussed in section 5.1 a shift in the size of the electron affinity of the supporting rare gas layer $E_{ea,Xe}$ is necessary. The peak positions of the cluster spectra still have a small deviation E_{add}, which can be explained with a screening effect of the partially into the rare gas layer penetrated clusters ΔE_C and a variation of the work function of the underlying material $\Delta\Phi_{HOPG}$.*

cluster anions measured in the gas phase lies the electron affinity $E_{\mathrm{ea,cl}}$ below the vacuum energy. An energy shift E_{C} between neutral clusters with $z = 0$ and cluster anions with $z = -1$ of

$$E_{\mathrm{C}} = \frac{e^2}{4\pi\epsilon(R+\delta)},$$

has to be taken into consideration to compare the spectra, as already mentioned in equation (2.2) on page 5. In table 5.2 the charging energy for different clusters is calculated. As discussed in section 5.1 a shift of the elec-

E_{C} / eV	$\mathrm{Cu_N}$	$\mathrm{Ag_N}$	$\mathrm{Fe_N}$
N = 34	2.58	2.33	2.58
N = 55	2.26	2.04	2.26
N = 90	1.96	1.76	1.97
N = 92	1.95	1.75	1.95
N = 147	1.70	1.53	1.70
N = 152	1.69	1.51	1.69
N = 309	1.36	1.22	1.37
N = 2000	0.77	0.68	0.77

Table 5.2: *Calculated charging energies for different clusters presented in this thesis with $\epsilon = 1 \cdot \epsilon_0$ and $\delta = 0.1\,nm$ substituted in equation (2.2) on page 5. It has to be mentioned that this approximation shows deviations for clusters with $R < 0.7\,nm$ and a decrease can be caused by a screening of a medium with $\epsilon > 1 \cdot \epsilon_0$ due to partially sunken clusters.*

tron affinity of the supporting rare gas layer $E_{\mathrm{ea,Xe}}$ has to be added. Even with the noted shifts there is still a small deviation between the peak positions of both spectra. A small change in the work function of the underlying material could be responsible for a deviation of the vacuum energy in our system. This leads to a shift of the gas phase cluster spectra $\Delta\Phi_{\mathrm{HOPG}}$, which is referenced to the vacuum energy. Another reason for the difference between the spectra could be a partial penetration of the clusters into the rare gas layers, which leads to a screening of the electric field and therefore a lowered charging energy ΔE_{C}. Additionally the approximation for the charging energy shows deviations for small clusters.
With the arrows in the top of Fig. 5.7 another approach to discuss the onset of the cluster spectra is added, which gets valid if the clusters are so large, that the density of states resembles bulk properties and only a size dependent correction for the ionization energy is needed.

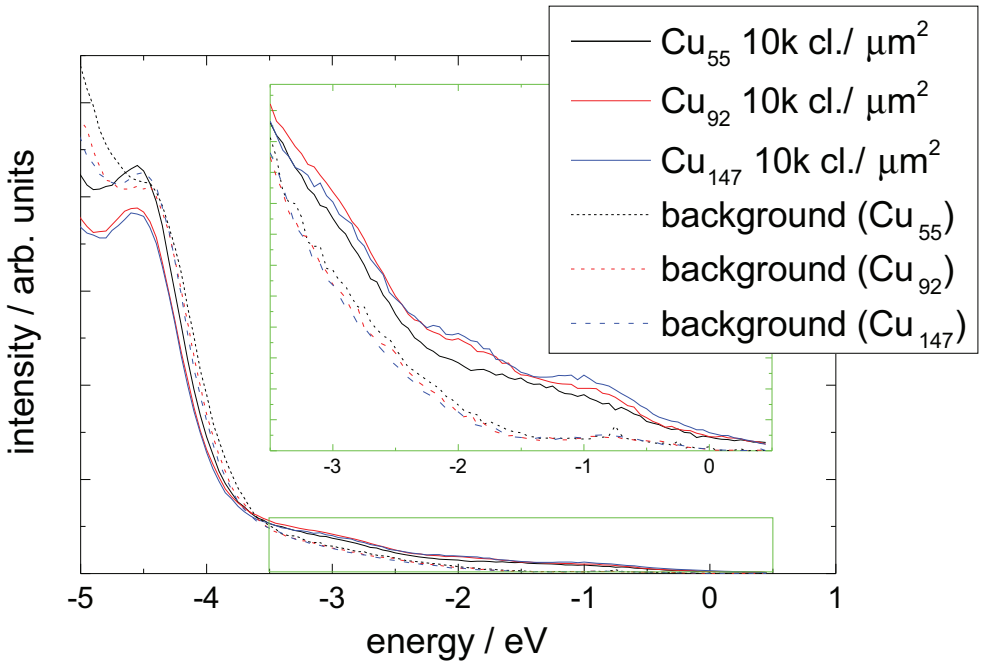

Figure 5.8: *UP spectra of Cu_{55}, Cu_{92} and Cu_{147} deposited on xenon adsorbed on HOPG and their corresponding background signal. The metal coverage changes the xenon $5p_{3/2}$ onset, which leaves only the region in the inset for proper evaluation. A size dependent change of the cluster signal can be observed.*

5.2.1 Copper clusters on xenon

An example for the measured data of copper clusters on xenon is shown in Fig. 5.8. 60 monolayers of xenon were adsorbed on HOPG and the measurements were performed at 25 K. All measurements before cluster deposition are plotted as dashed lines, which were smoothed with the Savitzky-Golay method, over 10 points and polynomial order of 2, to compensate the lower signal to noise ratio. The straight lines show the UP spectra after deposition. The onset of the $5p_{3/2}$ state of xenon is located 3.5 eV below the Fermi level. This peak shifts and changes in intensity with increasing metal coverage as already observed in [Pivetta, 2003; Pivetta et al., 2005] for copper and sodium on xenon. Because of that, only the region above -3.5 eV was evaluated, which is magnified in the inset. A size depending signal of the clusters can be seen in the s-p-band region. In order to extract the cluster signal each measurement was subtracted by its background signal, which is shown in Fig 5.9. The deposited Cu_{55} clusters show only one broad peak at

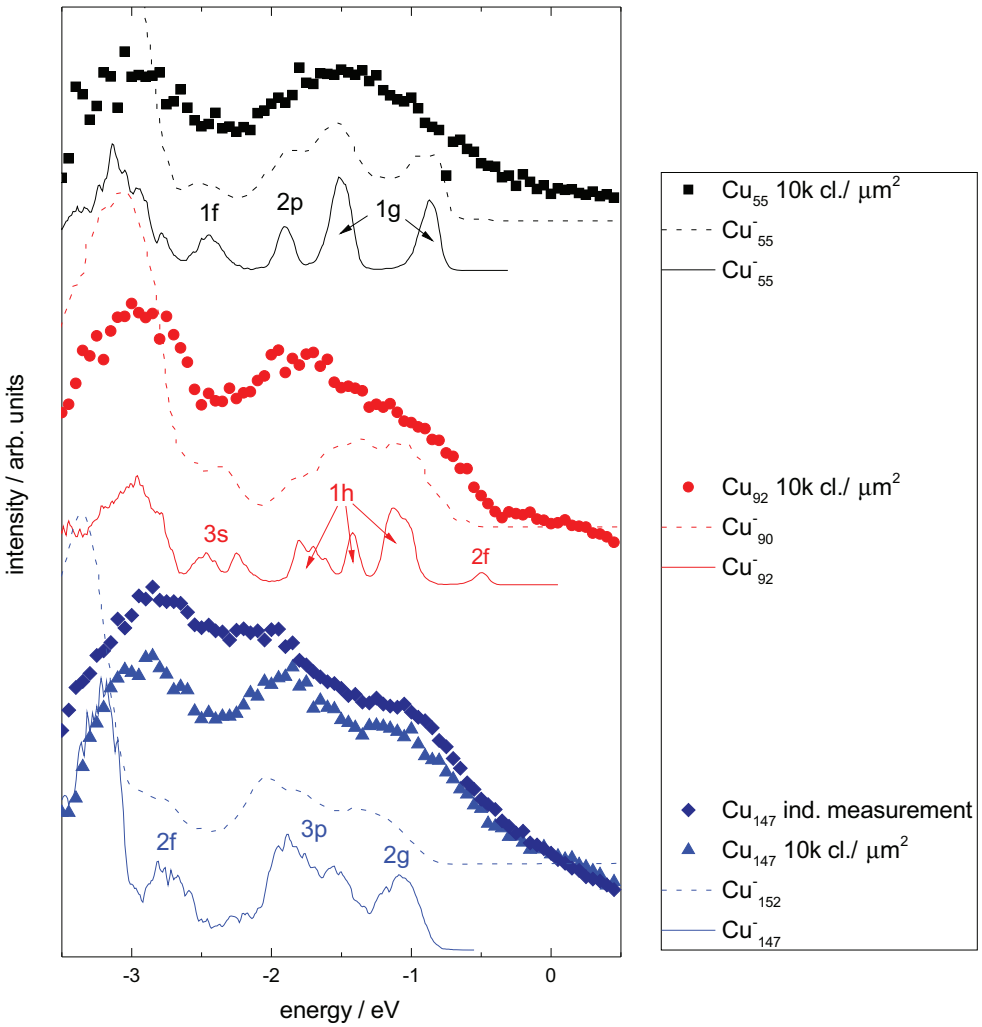

Figure 5.9: *The copper cluster signal extracted from the background signal for a comparison with the cluster spectra in the gas phase. For a better comparability the spectra are normalized. The UP spectra plotted with the dashed lines are from [Cheshnovsky et al., 1990; Taylor et al., 1992] and the straight lines from [Häkkinen et al., 2004; Kostko, 2007]. For Cu_{55} and Cu_{92} the accordance between the spectra is low due to the very broad structures of the deposited cluster spectra. The deposited Cu_{147} cluster spectra has a two peak structure similar to the gas phase measurements, which is verified by an independent measurement of a newly prepared sample.*

-1.50 eV in contrast to the three separated peaks of the measurements in the gas phase. For Cu_{92} there are two peaks at -1.80 eV and -1.05 eV, which might match with the outer 1h states of the gas phase measurements. In the case of Cu_{147} a striking accordance between the two peak structure at -1.90 eV and -1.10 eV with the 3p and 2g state occurs. In order to check the results a second independent measurement of a newly prepared sample with Cu_{147} was done, which verifies the two peak structure at -1.90 eV and -1.10 eV.
The UP spectra of clusters in the gas phase were shifted to fit the deposited cluster spectra, which results in a small additional shift corresponding to the shift $\Delta E_C + \Delta\Phi_{HOPG}$ in Fig. 5.7 of 0.45 eV for Cu_{55}, 0.50 eV for $Cu_{90,92}$ and 0.15 eV for $Cu_{147,152}$. The spectra with the straight lines are taken from [Häkkinen et al., 2004; Kostko, 2007] and the spectra plotted with dashed lines are from [Cheshnovsky et al., 1990; Taylor et al., 1992]. In these references the experimental setup is described, but it has to be mentioned that the clusters of [Häkkinen et al., 2004; Kostko, 2007] were trapped in an ion trap to reduce the cluster temperature before the measurement. The spectra from [Cheshnovsky et al., 1990; Taylor et al., 1992] contain broader signals, which is caused by the inferior energy resolution, higher cluster temperature and the oxygen contamination of the clusters of up to 10 %.
For the example of Cu_{55} it can be shown that the main difference between the spectra of deposited clusters and clusters in the gas phase is a broadening of the signals. In Fig. 5.10 the UP spectra of deposited Cu_{55} clusters on xenon on HOPG are shown together with the UP spectra from [Häkkinen et al., 2004; Kostko, 2007] convoluted with a Gaussian function ($\sigma = 0.35$ and $\mu = 0$ eV). The shape of the s-p-band region of the convoluted spectra fits to the spectra of the deposited clusters. The disagreement between these curves regarding the cluster d-band might be a consequence of the subtraction of the cluster spectra and its background signal or the approach of the convolution is too simple to provide reliable results. Furthermore a small deviation of the signal intensities can be explained by a change in excitation probabilities due to a difference in the photon energy. The energetic position of the UP spectra is arranged accordingly to the procedure done for Cu_{147}, but with an additional shift of 0.45 eV. This might be due to a higher charging energy and therefore a greater influence of the screening effect and that the Cu_{55} clusters are too small for the approximation of the metal sphere model. It has to be mentioned that the additional shift is nearly compensating the shift from the electron affinity of the xenon.
To investigate the influence of the underlying substrate further measurements of Cu_{147} were performed on Cu(111) and Au(111). The spectra of the deposited clusters are shown in Fig. 5.11, also the spectra of clusters in the gas phase are presented to compare the energetic position of the peaks. All measurements

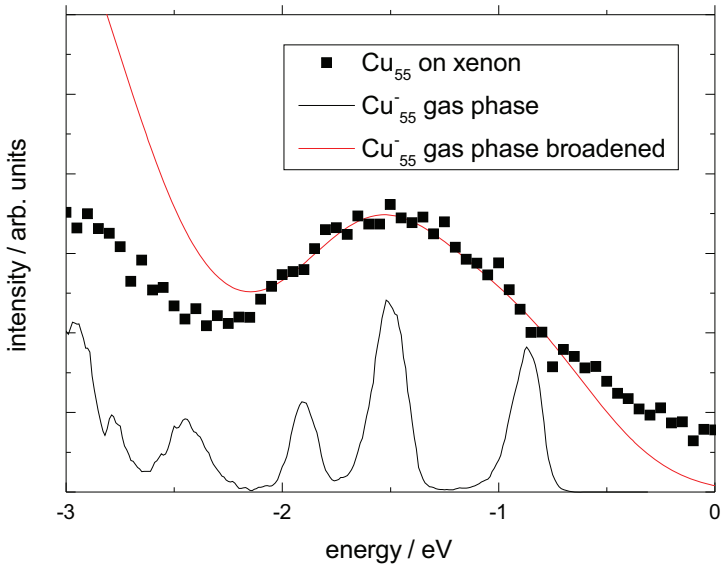

Figure 5.10: *The spectra of Cu_{55}^- in the gas phase is convoluted with a Gaussian function in order to fit the deposited cluster spectra. For the s-p-band an agreement between the spectra was accomplished.*

show a similar two peak structure, but the most pronounced peaks can be found on HOPG. The shift between these spectra can be explained by the difference in the work functions of the substrates, but the small additional shift of 0.15 eV on HOPG is changed to -0.20 eV for Cu(111) and Au(111). A second measurement on Cu(111) with a higher cluster coverage shows the same results, which proves that 10k clusters on a μm^2 is far below the coalescence threshold. It has to be mentioned that the least pronounced two peak structure are measured on xenon on gold, the same substrate for which the outlying measurements of C_{60} were observed. This suggests an interesting effect of xenon on gold.

Summary Cu_{55}, Cu_{92} and Cu_{147} were deposited on xenon adsorbed on HOPG. All measurements show features, which are broadened as compared to the free beam spectra. As reasons for this we suppose the energy resolution of 150 meV, differences in the geometry and a different penetration depth into the rare gas layers due to the velocity distribution of the cluster beam, which lead to a variety of differently screened charging energies. Especially for Cu_{147} the signal in the s-p-band of the deposited clusters is in accordance with the measurements performed in the gas phase. However, even the broad peaks can be matched to the gas phase spectra, which was shown by a

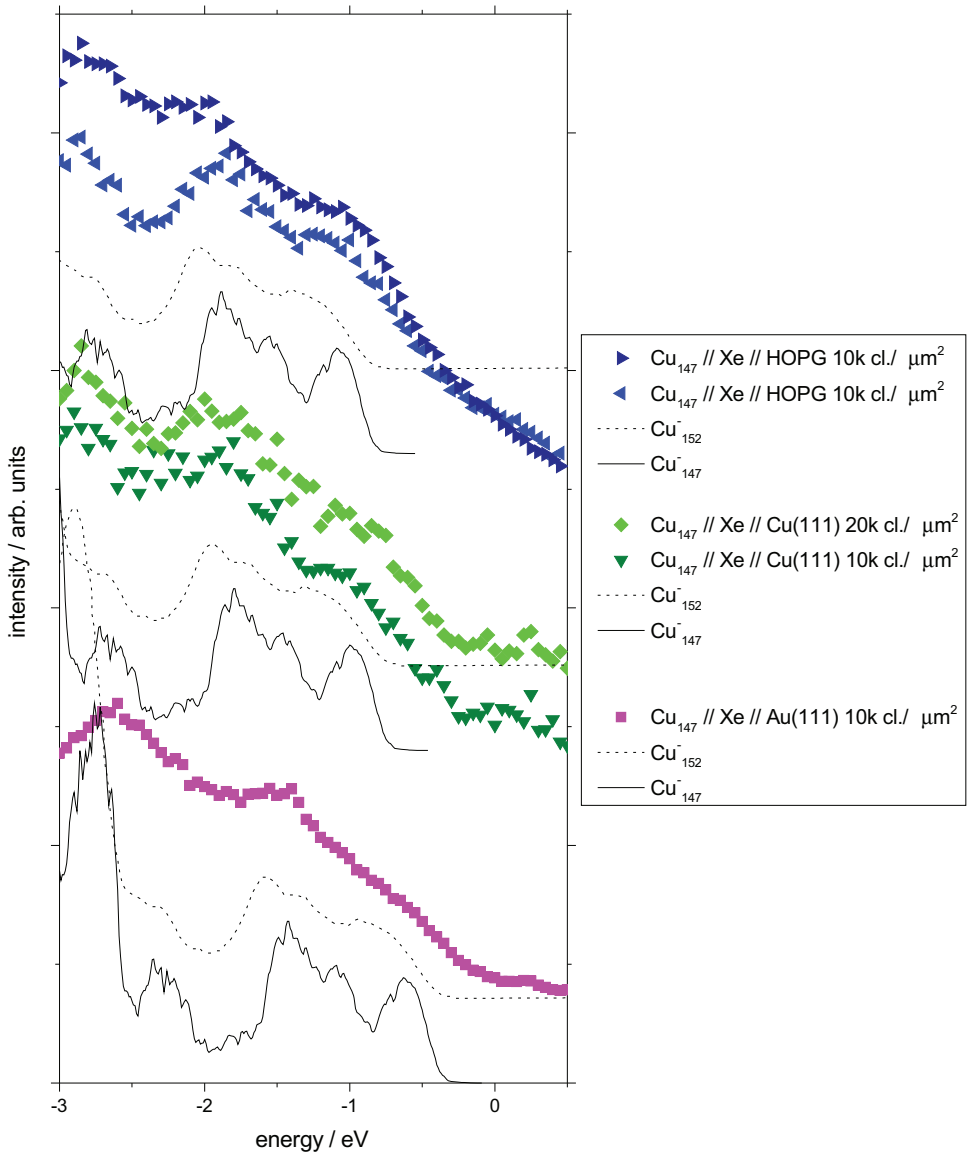

Figure 5.11: *A comparison of the spectra of all measurements of Cu_{147} on xenon with HOPG (25 K), Cu(111) (20 K) and Au(111) (20 K) as substrate. For an exact match of the spectra an additional shift for the clusters on Cu(111) and Au(111) of -0.20 eV and on HOPG of 0.15 eV has to be applied. The two peak structure was found on all substrates, especially on HOPG and Cu(111).*

comparison of deposited Cu_{55} clusters and the convolution of a Gaussian function with the gas phase spectra. Independent measurements for Cu_{147} of a newly prepared sample, measurements with a variation of the cluster coverage and two measurements on different substrates were performed to verify these results. Also the influence of the substrate on the spectra could be investigated simultaneously.

5.2.2 Copper clusters on argon and krypton

Copper clusters were also deposited, as described in chapter 4, on krypton and argon layers.

For a better understanding of how deep the clusters penetrate into the rare gas layers 2 ML of argon were adsorbed on Cu_{309} clusters deposited on argon, in order to obtain a spectra with clusters completely coated with argon. This is shown in Fig. 5.12 with a coverage of 10 k clusters per μm^2. The two UP spectra of not covered clusters were recorded three and eight hours after deposition and the background signal is already subtracted. In comparison the main difference between the cluster signals is a loss of intensity over time. Immediately after the measurements additional 2 ML argon were adsorbed and the sample was measured again. The cluster signal vanishes completely after the adsorption of only 2 ML argon. This indicates that the cluster on xenon and the C_{60} on all rare gases penetrated only partially or not at all into the rare gas layers, because the signal of the clusters remains during the measurements.

For smaller clusters, here Cu_{55}, on argon the UP spectra were measured and a change over time was noticed as shown in Fig. 5.13. The first spectrum roughly 385 s after deposition, shows a broad single peak structure comparable to the signal of Cu_{55} on xenon. In the course of time the broad peak vanishes and the remaining feature is similar to the signal of completely sunken clusters, as it was shown in Fig. 5.12. This behavior was already observed for silver clusters on xenon by [Ohno et al., 1991] and it was found that it occurs particularly on rare gas layers at higher temperatures due to van der Waals forces. This leads to the conclusion that even the sample temperature of 12 K is not low enough to investigate copper clusters on an argon layer. The circumstances for krypton are nearly the same and lead to the same conclusion.

In order to compare the shift of clusters to the shift of C_{60} on rare gas layers, high coverages of Cu_{309} clusters were deposited on xenon, krypton and argon as shown in Fig. 5.14. The d-band positions are marked with the dotted

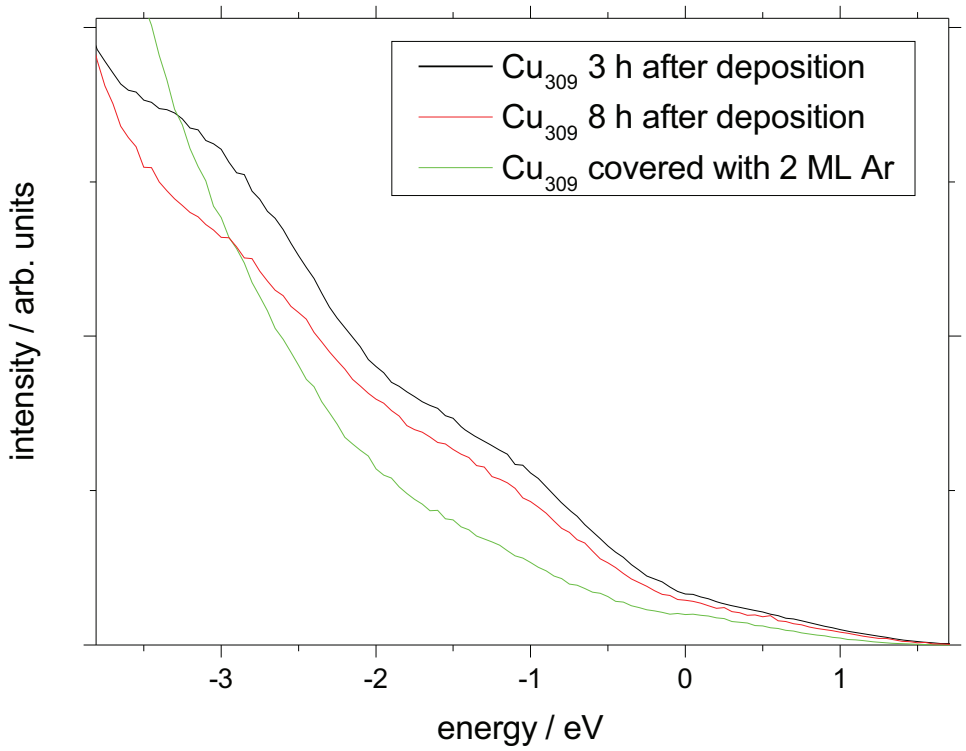

Figure 5.12: *Two UP spectra of Cu_{309} deposited on argon with a loss of intensity of the cluster signal over time. The adsorption of two further monolayers of argon on top of the clusters to coat the clusters in argon leads to a completely vanished cluster signal. The coverage is 10 k clusters per* μm^2.

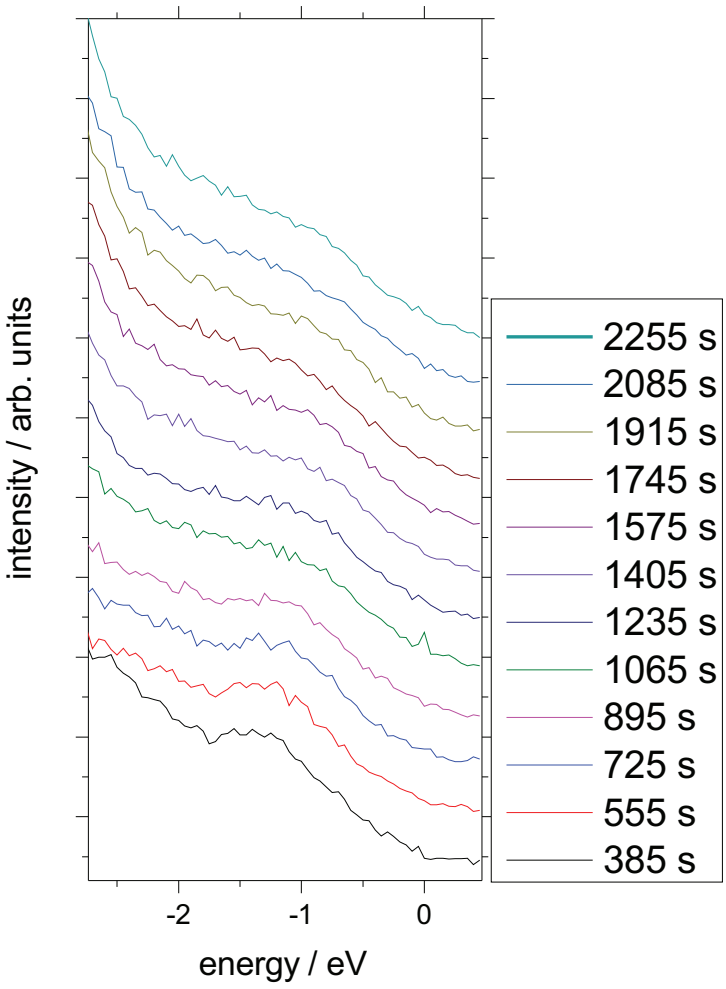

Figure 5.13: *UP spectra of Cu_{55} clusters deposited on argon on Ag(111) subtracted by the background signal. The time label for each curve is the duration between the deposition and the measurement. An offset in intensity was added to the UP spectra for a better comparability. The cluster signal vanishes over time, which indicates a sinking of the clusters into the rare gas layer probably due to a too high sample temperature.*

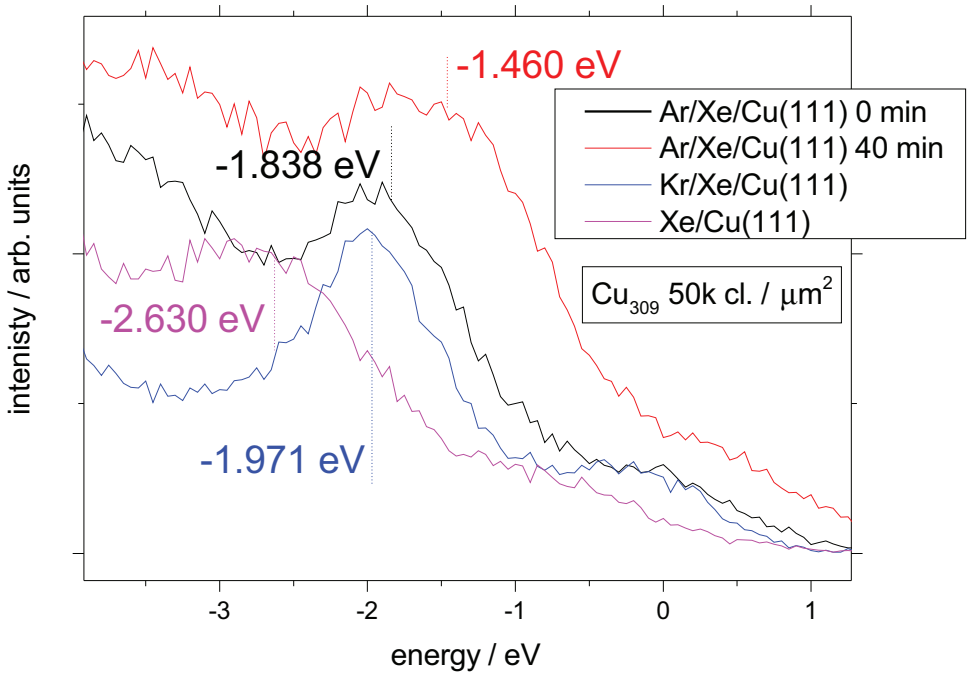

Figure 5.14: *Copper clusters with a high coverage of 50 k cl. / μm^2 were deposited on various rare gas layers on Cu(111) at 12 K. The time label for the two curves is the duration after the measurement started, whereas the deposition was roughly 5 min before. The peak positions of the d-bands are determined by fitting Gaussian functions with a linear background and marked to compare the differences with the expected values from the C_{60} experiment. The shift of the clusters on argon is in good agreement with the electron affinity of argon. The differences of the peak positions and the electron affinities of the rare gas layers show small deviations, which are in the magnitude of the resolution.*

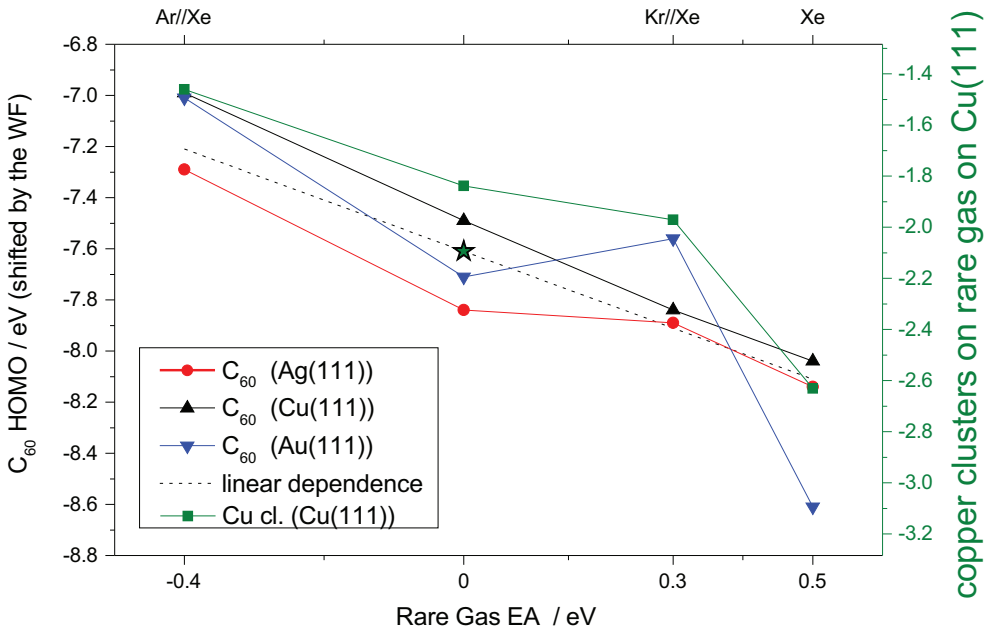

Figure 5.15: *The experimental data from section 5.1 of Fig. 5.6 on page 35 is extended by the copper d-band positions from Fig. 5.14 and the not saturated C_{60} measurements on argon at 0 eV. The star marks the d-band position of a polycrystalline copper bulk besides the HOMO peak position of free C_{60}. On all rare gas layers the same behavior for the copper clusters as for C_{60} molecules can be observed. The offset of 0.26 eV can be explained by the charging energy of large clusters with $R \approx 5\,nm$ due to coalescence or smaller clusters, which are screened by the rare gas layer.*

lines and show that the difference between the spectra is approximately the difference of their electron affinities. There is a time dependent shift of the d-band peak on argon of about -0.378 eV, which is within the limits of our resolution equal to the electron affinity of argon (-0.4 eV) and was already observed for C_{60} on argon. The distance between the d-band positions of the saturated argon measurement to the measurement on xenon is 1.170 eV, which is comparable to the difference of the electron affinities of 0.9 eV. The difference between the d-band peaks on krypton and the saturated argon signal is 0.511 eV, which is close to the difference of the electron affinities of 0.7 eV. A reason for the deviations can be the broad peaks and a decrease of the charging energy by coalescence and sinking of the clusters. In Fig. 5.15 the results from Fig. 5.6 on page 35 are extended by the d-band positions of the Cu_{309} clusters. The d-band positions of the copper clusters are referenced

to the green star, marking the d-band position of a cluster with $R \to \infty$ extracted from the polycrystalline copper spectra in Fig. 2.8 on page 11 of -2.094 eV below the Fermi energy. At 0 eV the not saturated d-band and HOMO positions on argon are marked in addition to Fig. 2.8 on page 11, which corresponds to neutral clusters as discussed in section 5.1. The curve for the high coverage of Cu_{309} clusters corroborates the effect observed for C_{60} on rare gas layers. The small offset of 0.26 eV for both data points on argon can be explained by the charging energy of coalesced clusters with $R \approx 5\,\text{nm}$, due to the high coverage, or by the charging energy of smaller clusters which are partially sunken and therefore screened by the rare gas layer. The deviations for krypton and xenon are similar to the C_{60} data.

Summary It was shown that a sample temperature of 12 K is not low enough to perform measurements of small copper clusters on argon or krypton, because of a sinking of the clusters into the rare gas layer. A verification of the shift observed for C_{60} was achieved by the comparison of Cu_{309} clusters deposited with high coverages on xenon, krypton and argon with the data of the HOMO positions of the C_{60} molecules.

5.2.3 Silver and iron clusters on xenon

Further measurements of silver and iron clusters, deposited on 60 ML xenon adsorbed on Ag(111) and Cu(111) at 15 K and 12 K, respectively, were performed.

In Fig. 5.16 Ag_{55}, Ag_{92} and Ag_{147} clusters on xenon are shown and compared to spectra of clusters in the gas phase from [Häkkinen et al., 2004; Kostko, 2007]. In order to fit the gas phase spectra to the deposited cluster spectra, a convolution of a Gaussian function with the gas phase spectra is plotted. The Gaussian root mean square widths of $\sigma_{\text{Ag}_{55}} = 0.30\,\text{eV}$, $\sigma_{\text{Ag}_{92}} = 0.40\,\text{eV}$ and $\sigma_{\text{Ag}_{147}} = 0.35\,\text{eV}$ were needed for a good agreement but no additional shift $E_{\text{add}} = \Delta E_{\text{C}} + \Delta\Phi$ (see Fig. 5.7). The absence of the additional shift can be explained by less sensitivity to small shifts due to the broadening of the spectra but also by the lower sample temperatures used for silver clusters of 15 K in contrast to copper clusters on xenon of 20 K to 25 K. This verifies the assumptions for the shift of molecules or clusters on rare gas layers.

Iron clusters deposited on xenon with 55, 147 and 2000 atoms were measured at 12 K as shown in Fig. 5.17. The cluster spectra in the gas phase are from [Wang et al., 2000] and measured with a photon energy of $\hbar\omega = 6.424\,\text{eV}$. In [Wang et al., 2000] there was no notable change between the Fe_{34}^- cluster and

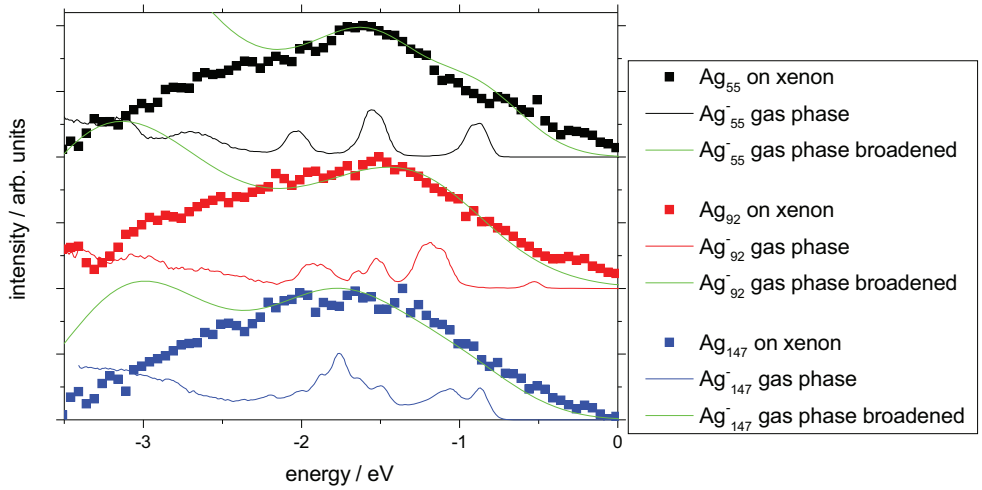

Figure 5.16: *The spectra of Ag_{55}^-, Ag_{92}^- and Ag_{147}^- in the gas phase were convoluted with Gaussian functions in order to fit the deposited cluster spectra. For the s-p-band an agreement between the spectra was accomplished without any additional shift. The clusters were deposited on xenon on Ag(111).*

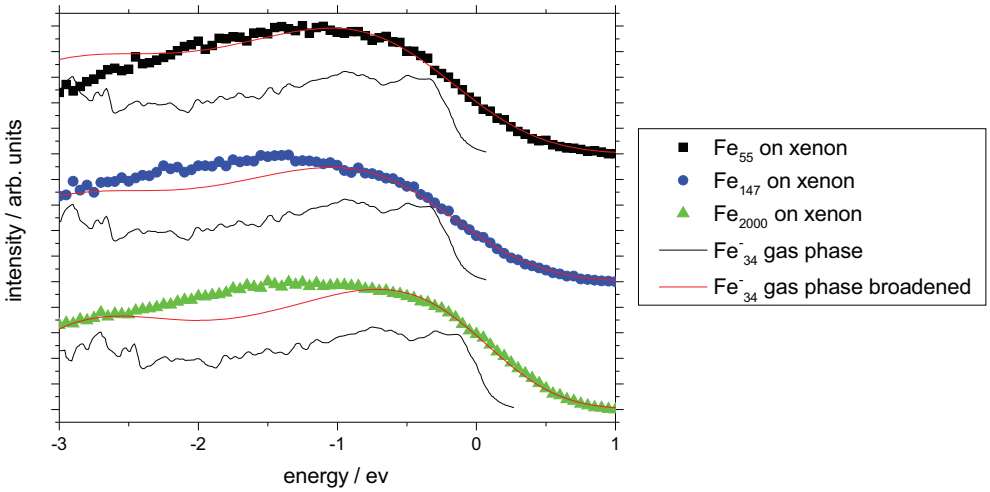

Figure 5.17: *Fe_{55}, Fe_{147} and Fe_{2000} clusters were deposited on xenon on Cu(111) and measured with UPS. For a comparison the convolution of the gas phase spectra ($\hbar\omega = 6.424\,\mathrm{eV}$) of Fe_{34}^- with a Gaussian function is shown. The onset of the cluster spectra are at the Fermi level, which might indicate a coupling of the clusters with the substrate.*

the bulk spectra, therefore no larger cluster sizes were measured. In order to fit the onset of the deposited cluster spectra the gas phase spectra were broadened and shifted, which results in the parameters listed in table 5.3. A

cluster	E_{add} / eV	σ / eV	onset / eV
Fe_{55}	0.37	0.5	-0.16
Fe_{147}	0.13	0.5	-0.16
Fe_{2000}	-0.01	0.4	0.11

Table 5.3: *The additional shift E_{add} and the Gaussian root mean square width σ needed to fit the measured iron cluster spectra. The onset of the shifted spectra is determined as inflection point.*

correction of the shift due to the size dependent charging energy difference of the deposited clusters to the Fe_{34} clusters according to equation 2.1 on page 4, with $\alpha \approx 0.42$ from Ref. [Seidl et al., 1998], was applied. The broadened gas phase and the deposited cluster spectra show nearly no structure except for the step edge of the d-band. Therefore only the position of this onset was analyzed. For Fe_{2000} the onset of the cluster d-band is in good agreement to the cluster gas phase spectra with no additional shift. In the case of Fe_{55} and Fe_{147} a small additional shift E_{add} was needed to align the onsets of the spectra. The additional shift increases with decreasing cluster size, probably due to the screening of the charging energy for smaller clusters.

Chapter 6

Outlook

This chapter starts with a brief compilation of three further sample options for metal cluster deposition. The chosen variant for following experiments will be described from the preparation to first results.

6.1 Other sample options

In order to perform experiments on clusters usable for applications a room temperature stable sample system would be desirable. To retain mass-selected clusters on the surface, the cluster diffusion has to be avoided. One route is to capture the clusters on periodically ordered active surface sites, which enables more applications such as data storage, electrical transport or catalysis.
In Ref. [Weiss et al., 2005] the magnetization of Co nanoparticles self-assembled on a Au(788) surface are presented. This gold surface shows a superlattice of favorable (111) microfacets, which serve as nucleus of growth to arrange the magnetic clusters.
A Graphene layer on Ir(111) was used by [N'Diaye et al., 2006] to form a two-dimensional Ir cluster array by the growth of Ir nanoparticles. The favorable sites on this surface are created by a Moiré pattern due to the overlay of the two periodic lattices. A similar surface system of graphene on Ru(0001), which also forms a Moiré pattern, was used by [Wang et al., 2012] for the deposition of mass-selected $Pd_{N<20}$ clusters. In the work of [Riedl et al., 2009] quasi-free-standing graphene on SiC(0001) using hydrogen intercalation to decouple the graphene from the SiC(0001) surface is shown, which might decrease the cluster substrate interaction even further.
The approach of [Degen et al., 2004] are thin alumina films on $Ni_3Al(111)$, which will be the topic of the following section.

6.2 Thin Al_2O_3 films on $Ni_3Al(111)$

As already mentioned, a $Ni_3Al(111)$ crystal was used as substrate. By oxidation, two Al_2O_3 monolayers were grown on the surface. Depending on the tunneling voltage different structures get visible in STM images. A *network structure* with a lattice vector length of 2.40 nm and a *dot structure* with a lattice vector length of 4.16 nm are the superstructures imaged in STM with a $(\sqrt{3} \times \sqrt{3})$ R30° relation to each other. Although the exact geometric surface structure is uncertain, the *dot structure* can be identified as electronic and structural defects, which serve as nuclei for cluster formation [Degen et al., 2005].
It was already shown that clusters are formed with a broad size distribution and arranged in arrays on the surface by adsorbed metal atoms [Becker et al., 2002]. Our approach is to deposit mass-selected clusters on the surface in order to obtain an array of clusters with a very narrow size distribution. The first issues to investigate will concern temperature and size depending mobility of the clusters.

6.2.1 Preparation

The preparation procedure of the sample consists of heating, sputtering and oxidization processes and is described in [Degen, 2005]. For the sputtering process the argon sputter gun described in chapter 3 was used. The oxygen inlet for the oxidization process needs to be baked out before operation to avoid any further contamination of the oxygen with a purity of 99.998 %.
The heatable sample holder installed in the manipulator does not meet the requirements needed for the preparation. A base pressure below $3 \cdot 10^{-9}$ mbar while the sample is heated up to 1200 K is needed. These criteria leaded to the construction of a new heating station. An illustration is shown in Fig. 6.1. A filament can be heated with a current of up to 4.3 A to eject electrons. The high voltage of up to 1200 V applied between the filament and the sample accelerates the electrons on the backside of the sample to heat it with electron impact. Al_2O_3 ceramic components decouple the sample holder and filament electrically and thermally from the rest of the heating station. In practice a small voltage is applied between the grounded part of the heating station and the filament to prevent the electrons from reaching the ionization vacuum gauge, which otherwise leads to an error in the measured pressure. To reduce the radiated power of the filament a shield is installed above it. For a low heat exchange the sample is mounted with a wire on a sample plate with a hole and just three small webs as contact faces. The sample temperature is measured contactless by an infrared pyrometer with a temperature range

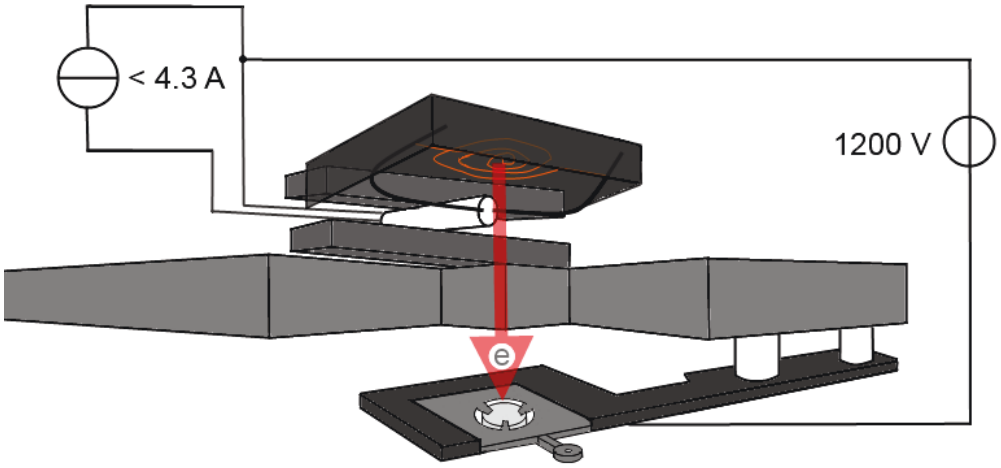

Figure 6.1: *A sketch of the heating station build to heat samples over 1200 K with a low pressure increase. The tungsten filament, shown in orange, is heated by a current source with up to 4.3 A to provide free electrons. A high voltage of about 1200 V accelerates the electrons on the backside of the sample to heat it by electron impact. A shield is installed above the filament to reduce the radiated power. To restrict the heated material the sample holder and the filament are thermally decoupled from the other parts of the heating station.*

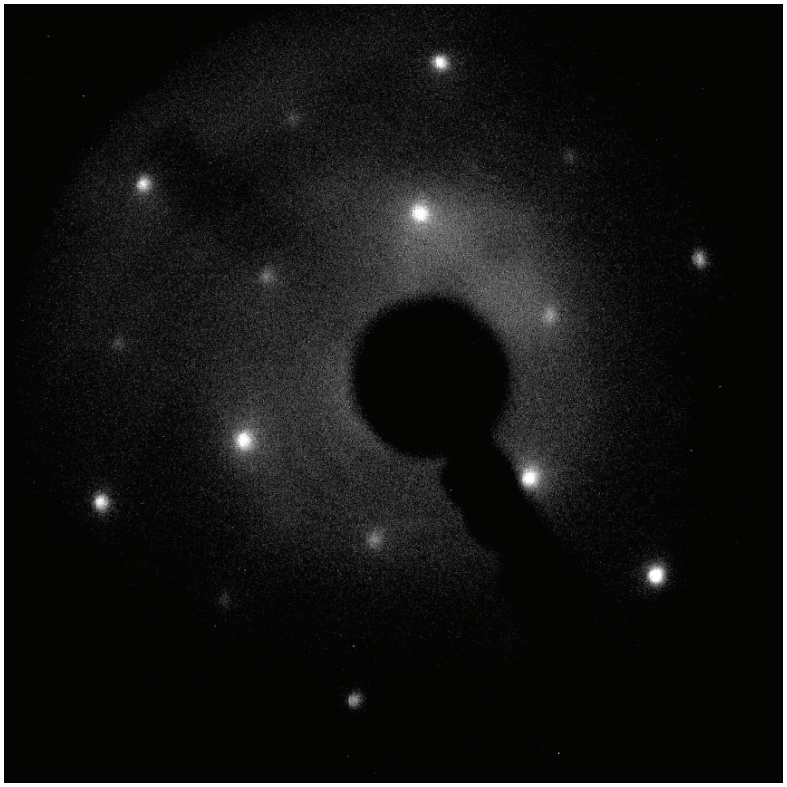

Figure 6.2: *LEED image of the cleaned $Ni_3Al(111)$ crystal measured with a kinetic energy of 93 eV at room temperature.*

from 658 K to 1873 K, a measurement spot of 1.5 mm at 450 mm distance and a spectral response of 1.6 µm. The heating parameters to reach the same temperature vary too much for different experimental runs, which makes the temperature control during each heating step inevitable.

In order to prepare the $Ni_3Al(111)$ crystal for the oxidization procedure the sample was sputtered for 30 min with 5.2 $\mu A/cm^2$ by argon ions to remove oxides and adsorbates. In order to anneal and enrich the surface with aluminum the sample was heated to 1150 K for 7 min and subsequently to 1000 K for 7 min, which leads to a segregation of the aluminum atoms to the surface. These two process steps were repeated until the LEED image shows hexagonal features, as presented in Fig. 6.2.
The cleaned $Ni_3Al(111)$ crystal was oxidized in the heating station. While the sample was at 1000 K, oxygen was let into the analysis chamber to a pressure of $3 \cdot 10^{-8}$ mbar for 1773 s. A base pressure of $3 \cdot 10^{-9}$ mbar of the residual gases during oxidization should not be exceeded to obtain a high quality oxide

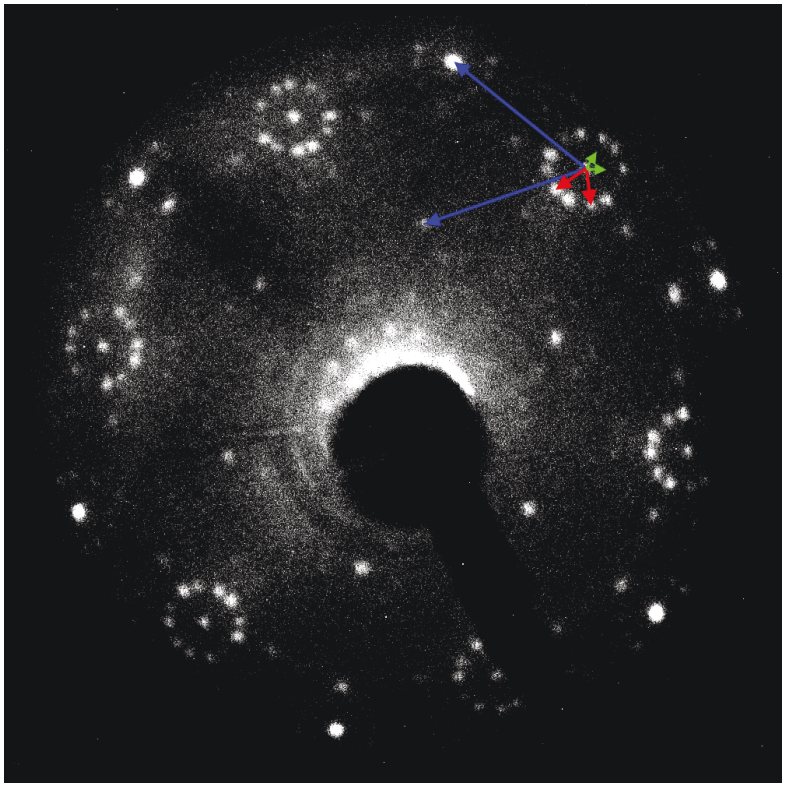

Figure 6.3: *A LEED measurement of the oxidized $Ni_3Al(111)$ crystal measured with a kinetic energy of 79.3 eV at room temperature, which formed two monolayers of Al_2O_3. The reflexes corresponding to the unit cell of the substrate are marked with blue arrows. The network structure is marked with red arrows and the green arrows mark the positions where the reflexes of the dot structure should be.*

film. This was checked by observing the pressure, while the sample was at 1000 K for 1773 s without oxygen exposure. After the oxidization step, the sample was heated to 1050 K for 300 s. These process steps were repeated until the LEED image shows features as in Fig. 6.3, which is commonly the case after two cycles. Two monolayers of Al_2O_3 were formed on the surface. The reflexes marked with the blue arrows are corresponding to the unit cell of the substrate. There are twelve spots around these reflexes, here marked with red arrows, indicating that there are two superstructures with an edge length of 2.40 nm 24° rotated to each other, which are called *network structure*. As shown in [Degen, 2005], there should be twelve further reflexes corresponding to a pair of *dot structures* with an edge length of 4.16 nm and a rotation to each other of 24° at the positions marked with the green arrows, which are not

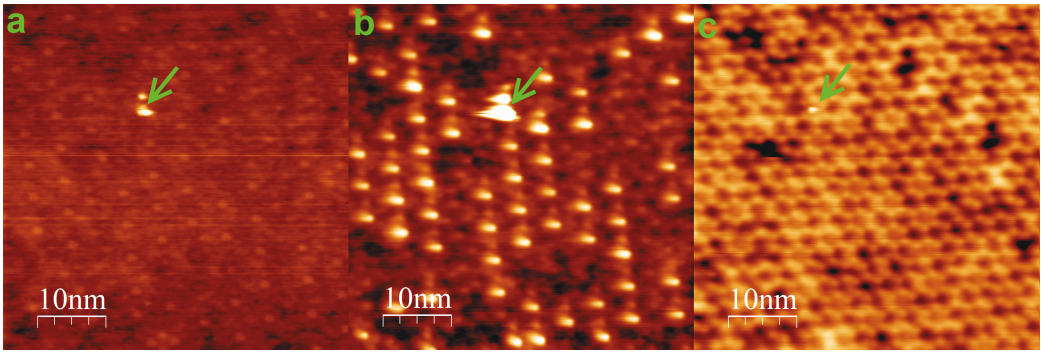

Figure 6.4: *Three STM images of the same* $50 \times 50\,nm^2$ *spot (this gets visible by the point defect marked with an arrow) on the oxidized* $Ni_3Al(111)$ *crystal measured with a current of 0.1 nA and three different voltages (a =* $0.7\,V$*,* $b = 2\,V$ *and* $c = 3.2\,V$*). At 0.7 V the flat surface is imaged. Because of the electronic active sites of the superstructures, the dot structure can be seen at 2 V and the network structure at 3.2 V. A defect rich surface was chosen for an easier comparison of the images.*

noticeable in this measurement. After two oxide monolayers are formed the oxidization process stops self-limiting regardless of further oxygen exposure. Three STM images of the Al_2O_3 structure on $Ni_3Al(111)$ are shown in Fig. 6.4. All measurements were performed at $T = 77\,K$ on the same $50 \times 50\,nm^2$ spot with 0.1 nA feedback current and three different gap voltages. To visualize the surface geometry a voltage of 0.7 V (a) is suitable. Due to the electronic active defects from the superstructure, the *dot structure* can be visualized at 2 V (b) and the *network structure* at 3.2 V (c).

6.2.2 First results for cluster deposition

Cu_{55} clusters were deposited on the surface of the thin Al_2O_3 film on $Ni_3Al(111)$ at 77 K and investigated with STM in Fig. 6.5. Further investigations of the mobility of copper clusters deposited with different sizes and at different temperatures will be done. Spectroscopic measurements with the combination of STS and UPS will be used to analyze the electronic structure of the clusters and the influence of the surface on it. The deposition of iron clusters on this system might be of importance, due to applications for arranged magnetic moments.

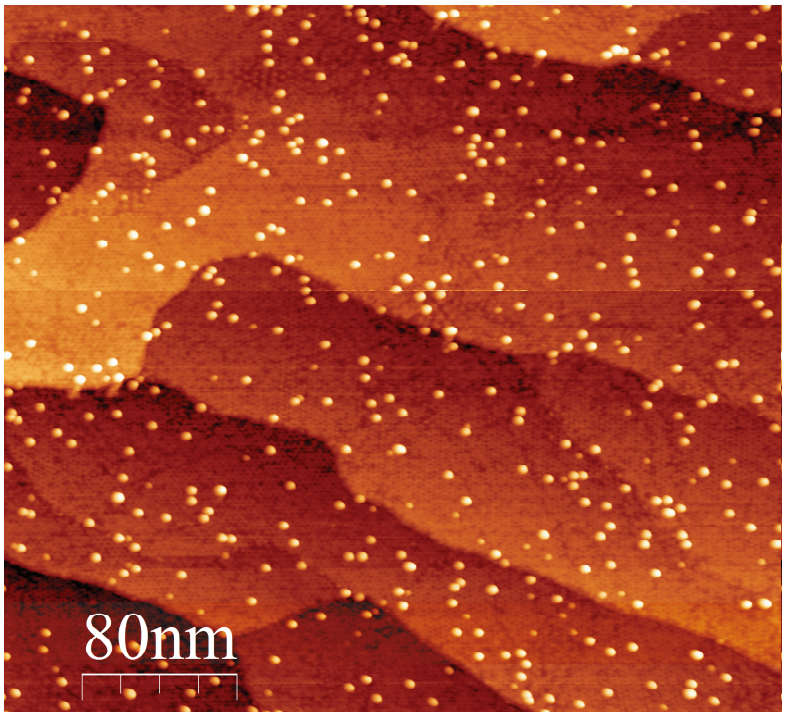

Figure 6.5: *A STM image of Cu_{55} clusters deposited on thin Al_2O_3 film on $Ni_3Al(111)$ at 77 K with 0.1 nA and 3.5 V.*

Chapter 7

Summary

The rare gas adsorption performed with the two step process produced well ordered and flat rare gas layers, verified by UPS and LEED measurements. With this spacer layer molecules and clusters could be decoupled from the substrate.

C_{60} molecules were measured with UPS on nine different sample systems, combining xenon, argon and krypton as rare gas layers with Cu(111), Ag(111) and Au(111) as substrates. The energetic positions of the HOMO were evaluated to determine the shift of the spectra on different samples. A shift of the UP spectra by the electron affinity of the rare gas layer to lower energies was necessary to fit the recorded data. The spectra on argon showed a shift on time scales of 3000 s and an increasing intensity of the LUMO+1 state, which suggests that a charge transfer to the molecules is the reason for the shift of the spectra. Additionally the shift of the HOMO of C_{60} on argon started at 0 eV and ended roughly at 0.4 eV, the difference being exactly the electron affinity of argon. For xenon and krypton the time scale of the shift is too short, thus only the final shift was observed.

Copper clusters with 55, 92 and 147 atoms were soft-landed on xenon on HOPG and the UP spectra showed a sized dependent signal in the s-p-band region of the clusters. A comparison between the spectra of deposited clusters and the gas phase experiments from [Häkkinen et al., 2004; Kostko, 2007; Cheshnovsky et al., 1990; Taylor et al., 1992] yielded a good agreement for Cu_{147} clusters. For Cu_{55} and Cu_{92} clusters the match between the deposited and gas phase spectra was worse, which might be due to a broadening of the deposited cluster spectra. It was shown that by a convolution of the gas phase Cu_{55} cluster spectra with a Gaussian function a good agreement with the deposited cluster spectra can be obtained. This broadening of the spectra also

leaded to good accordance for deposited silver clusters with 55, 92 and 147 atoms to the gas phase spectra. The shift of the spectra fitted to the results obtained for C_{60} with small deviations for copper clusters and no deviation for silver clusters. In the case of iron clusters with 55, 147, and 2000 atoms unstructured spectra, as expected by the gas phase spectra, were shown. The position of the d-band onset was in agreement to the shifts observed for C_{60} with a deviation for smaller clusters due to screening effects. Cu_{309} clusters were deposited on argon on xenon and covered with two more argon layers, which results in a complete vanishing of the cluster signal in the UP spectra. This indicates that the C_{60} molecules on xenon, krypton and argon and the copper clusters on xenon are not sinking into the rare gas layer, because of the unchanged cluster signal. For copper clusters on argon or krypton no reliable data was recorded, probably due to too high sample temperatures and therefore a quick sinking into the rare gas.

The preparation of thin Al_2O_3 layers on $Ni_3Al(111)$ surfaces was presented in detail. A heating station was constructed for the special requirements of the sample preparation. LEED and STM images showed the *network structure* and especially the *dot structure*, which provides active sites in order to obtain room temperature stable clusters at defined positions. First measurements on deposited mass-selected clusters on this sample system were shown.

The change of the ionization potential of molecules and other nanostructures on rare gas layers can be of great importance if it is transferable to other isolating or even semi conductive sample systems. To gain a deeper understanding together with additional experimental data a theoretical modelling of the charging effect would be useful.

Quantized states of deposited clusters are interesting for a variety of applications. A room temperature stable system with low cluster surface interaction would be needed for real-life applications of the cluster properties as investigated in the gas phase. The thin oxide layer might be a suitable surface environment, because of the low cluster surface interaction together with the active sites which arrange the clusters in an array. The next step will be the investigation of small metal cluster on a thin Al_2O_3 layers on a $Ni_3Al(111)$ crystal with a combination of UPS, as an averaging method, and STS, as a single cluster measurement. Further studies of iron clusters as magnetic moments arranged in arrays will be done.

Bibliography

Albrektsen, O., H. W. M. Salemink, K. A. Mørch, and A. R. Thölen: 1994, 'Reliable tip preparation for high-resolution scanning tunneling microscopy'. *Journal of Vacuum Science & Technology B* **12**(6), 3187–3190.

Becker, C., A. Rosenhahn, A. Wiltner, K. von Bergmann, S. J., P. Pervan, M. Milun, M. Kralj, and K. Wandelt: 2002, 'Al2O3-films on Ni3Al(111): a template for nanostructured cluster growth'. *New Journal of Physics* **4**(1), 75.

Berglund, C. N. and W. E. Spicer: 1964a, 'Photoemission Studies of Copper and Silver: Experiment'. *Phys. Rev.* **136**, A1044–A1064.

Berglund, C. N. and W. E. Spicer: 1964b, 'Photoemission Studies of Copper and Silver: Theory'. *Phys. Rev.* **136**, A1030–A1044.

Brack, M.: 1993, 'The physics of simple metal clusters: self-consistent jellium model and semiclassical approaches'. *Rev. Mod. Phys.* **65**, 677–732.

Budke, M. and M. Donath: 2008, 'Ar gas discharge lamp with heated LiF window: A monochromatized light source for photoemission'. *Applied Physics Letters* **92**(23), 231918.

Cheshnovsky, O., K. J. Taylor, J. Conceicao, and R. E. Smalley: 1990, 'Ultraviolet photoelectron spectra of mass-selected copper clusters: Evolution of the 3 d band'. *Phys. Rev. Lett.* **64**, 1785–1788.

Chou, M., A. Cleland, and M. L. Cohen: 1984, 'Total energies, abundances, and electronic shell structure of lithium, sodium, and potassium clusters'. *Solid State Communications* **52**(7), 645 – 648.

Dederichs, P., H. Schober, D. Sellmyer, E. Fawcett, R. Griessen, W. Joss, W. Kress, and A. Cracknell: 1983, *Landolt-Börnstein - Group III: Crystal and Solid State Physics*, Vol. 13. Springer Berlin Heidelberg.

Degen, S.: 2005, 'Aufbau eines Tieftemperaturrastertunnelmikroskops und Messungen auf Ni3Al(111)'. Ph.D. thesis, Rheinischen Friedrich-Wilhelms-Universität Bonn.

Degen, S., C. Becker, and K. Wandelt: 2004, 'Thin alumina films on Ni3Al(111): A template for nanostructured Pd cluster growth'. *Faraday Discuss.* **125**, 343–356.

Degen, S., A. Krupski, M. Kralj, A. Langner, C. Becker, M. Sokolowski, and K. Wandelt: 2005, 'Determination of the coincidence lattice of an ultra thin Al2O3 film on Ni3Al(111)'. *Surface Science* **576**(13), L57 – L64.

DeMenech, M., U. Saalmann, and M. E. Garcia: 2007, 'Recovering hidden electronic states using energy-resolved imaging of metal clusters at surfaces'. *New Journal of Physics* **9**(9), 340.

Duffe, S.: 2009, 'Thermally activated processes and electronic properties of size selected Ag clusters and grown metal islands on C60 functionalized surfaces'. Ph.D. thesis, TU Dortmund, http://hdl.handle.net/2003/26100.

Feibelman, P. J. and D. E. Eastman: 1974, 'Photoemission spectroscopy - Correspondence between quantum theory and experimental phenomenology'. *Phys. Rev. B* **10**, 4932–4947.

Feynman, R.: 1960, 'There's Plenty of Room at the Bottom'. *Engineering and Science* **23:5**, 22–36.

Gimzewski, J. K. and R. Möller: 1987, 'Transition from the tunneling regime to point contact studied using scanning tunneling microscopy'. *Phys. Rev. B* **36**, 1284–1287.

Goldmann, A.: 2003, *Noble Metals, Noble Metal Halides and Nonmagnetic Transition Metals*, Vol. 23c1. Springer Berlin Heidelberg.

Green, W. H., S. M. Gorun, G. Fitzgerald, P. W. Fowler, A. Ceulemans, and B. C. Titeca: 1996, 'Electronic Structures and Geometries of C60 Anions via Density Functional Calculations'. *The Journal of Physical Chemistry* **100**(36), 14892–14898.

Grönhagen, N., T. T. Järvi, N. Miroslawski, H. Hövel, and M. Moseler: 2012, 'Decay Kinetics of Cluster-Beam-Deposited Metal Particles'. *The Journal of Physical Chemistry C* **116**(36), 19327–19334.

Haberland, H., C. Bahr, T. Dorfmüller, G. Heppke, S. Hess, H. Jockusch, K. Lüders, J. Seidel, R. Thull, H. Tschesche, and B. Wende: 1992, *Lehrbuch der Experimentalphysik*, Vol. 5. De Gruyter.

Haberland, H., M. Mall, M. Moseler, Y. Qiang, T. Reiners, and Y. Thurner: 1994, 'Filling of micron-sized contact holes with copper by energetic cluster impact'. *Journal of Vacuum Science & Technology A* **12**(5), 2925–2930.

Häkkinen, H., M. Moseler, O. Kostko, N. Morgner, M. A. Hoffmann, and B. v. Issendorff: 2004, 'Symmetry and Electronic Structure of Noble-Metal Nanoparticles and the Role of Relativity'. *Phys. Rev. Lett.* **93**, 093401.

Hoffmann, M. A., G. Wrigge, and B. v. Issendorff: 2002, 'Photoelectron spectroscopy of Al^-_{32000} : Observation of a "Coulomb staircase" in a free cluster'. *Phys. Rev. B* **66**, 041404.

Hüfner, S.: 2003, *Photoelectron Spectroscopy*. Springer Berlin Heidelberg.

Irawan, T., D. Boecker, F. Ghaleh, C. Yin, B. Von Issendorff, and H. Hövel: 2006, 'Metal clusters on rare gas layers - growth and spectroscopy'. *Applied Physics A* **82**(1), 81–86.

Klein, M. L. and J. A. Venables (eds.): 1977, *Rare Gas Solids*, Vol. II. Academic Press.

Knight, W. D., K. Clemenger, W. A. de Heer, W. A. Saunders, M. Y. Chou, and M. L. Cohen: 1984, 'Electronic Shell Structure and Abundances of Sodium Clusters'. *Phys. Rev. Lett.* **52**, 2141–2143.

Knorr, N., H. Brune, M. Epple, A. Hirstein, M. A. Schneider, and K. Kern: 2002, 'Long-range adsorbate interactions mediated by a two-dimensional electron gas'. *Phys. Rev. B* **65**, 115420.

Kostko, O.: 2007, 'Photoelectron spectroscopy of mass-selected sodium, coinage metal and divalent metal cluster anions'. Ph.D. thesis, Albert-Ludwig-Universität Freiburg.

Kostko, O., B. Huber, M. Moseler, and B. von Issendorff: 2007, 'Structure Determination of Medium-Sized Sodium Clusters'. *Phys. Rev. Lett.* **98**, 043401.

Li, W. and D. Y. Li: 2005, 'On the correlation between surface roughness and work function in copper'. *The Journal of Chemical Physics* **122**(6), 064708.

Lifshitz, C.: 1993, 'Energetics and dynamics of ionization and dissociation of fullerene carbon clusters'. *Mass Spectrometry Reviews* **12**(5-6), 261–284.

Lim, D.-C., C.-C. Hwang, G. Gantefor, and Y. D. Kim: 2010, 'Model catalysts of supported Au nanoparticles and mass-selected clusters'. *Phys. Chem. Chem. Phys.* **12**, 15172–15180.

Lüth, H.: 1993, *Surface and Interfaces of Solids*. Springer-Verlag.

Miroslawski, N.: 2010, 'Geometrisch und elektronisch magische Cluster'. Master's thesis, TU Dortmund.

Miroslawski, N.: 2013, 'Ultraviolet photoelectron spectroscopy and scanning tunnelling microscopy of silver and copper clusters on HOPG, noble metals and rare gas layers'. Ph.D. thesis, TU Dortmund.

N'Diaye, A. T., S. Bleikamp, P. J. Feibelman, and T. Michely: 2006, 'Two-Dimensional Ir Cluster Lattice on a Graphene Moiré on Ir(111)'. *Phys. Rev. Lett.* **97**, 215501.

Ohno, T. R., J. C. Patrin, U. S. Ayyala, and J. H. Weaver: 1991, 'Ag deposition onto Xe: Clustering, incorporation, and surface attraction'. *Phys. Rev. B* **44**, 1891–1895.

Peters, S., S. Peredkov, M. Neeb, W. Eberhardt, and M. Al-Hada: 2013, 'Size-dependent Auger spectra and two-hole Coulomb interaction of small supported Cu-clusters'. *Phys. Chem. Chem. Phys.* **15**, 9575–9580.

Pivetta, M.: 2003, 'Adsorbate-substrate interactions and electron confinement at surfaces'. Ph.D. thesis, Faculté des Sciences de l'Université de Lausanne.

Pivetta, M., F. Patthey, I. Barke, H. Hövel, B. Delley, and W.-D. Schneider: 2005, 'Gap opening in the surface electronic structure of graphite induced by adsorption of alkali atoms: Photoemission experiments and density functional calculations'. *Phys. Rev. B* **71**, 165430.

Riedl, C., C. Coletti, T. Iwasaki, A. A. Zakharov, and U. Starke: 2009, 'Quasi-Free-Standing Epitaxial Graphene on SiC Obtained by Hydrogen Intercalation'. *Phys. Rev. Lett.* **103**, 246804.

Schooss, D., M. N. Blom, J. H. Parks, B. v. Issendorff, H. Haberland, and M. M. Kappes: 2005, 'The Structures of Ag_{55}^{+} and Ag_{55}^{-}: Trapped Ion Electron Diffraction and Density Functional Theory'. *Nano Letters* **5**(10), 1972–1977.

Seidl, M., J. P. Perdew, M. Brajczewska, and C. Fiolhais: 1998, 'Ionization energy and electron affinity of a metal cluster in the stabilized jellium model: Size effect and charging limit'. *The Journal of Chemical Physics* **108**(19), 8182–8189.

Sessoli, R., D. Gatteschi, A. Caneschi, and M. A. Novak: 1993, 'Magnetic bistability in a metal-ion cluster'. *Nature* **365**, 141 – 143.

Sieben, B.: 2007, 'Rastertunnelmikroskopie an Clustersystemen'. Master's thesis, TU Dortmund.

Siekmann, H., B. Wrenger, E. Holub-Krappe, C. Pettenkofer, and K. Meiwes-Broer: 1993, 'Valence band photoemission from deposited metal clusters: Case studies'. *Zeitschrift für Physik D Atoms, Molecules and Clusters* **26**(1), 54–57.

Suga, S., A. Sekiyama, G. Funabashi, J. Yamaguchi, M. Kimura, M. Tsujibayashi, T. Uyama, H. Sugiyama, Y. Tomida, G. Kuwahara, S. Kitayama, K. Fukushima, K. Kimura, T. Yokoi, K. Murakami, H. Fujiwara, Y. Saitoh, L. Plucinski, and C. M. Schneider: 2010, 'High resolution, low hv photoelectron spectroscopy with the use of a microwave excited rare gas lamp and ionic crystal filters'. *Review of Scientific Instruments* **81**(10), 105111.

Taylor, K. J., C. L. Pettiette-Hall, O. Cheshnovsky, and R. E. Smalley: 1992, 'Ultraviolet photoelectron spectra of coinage metal clusters'. *The Journal of Chemical Physics* **96**(4), 3319–3329.

Tersoff, J. and D. R. Hamann: 1985, 'Theory of the scanning tunneling microscope'. *Phys. Rev. B* **31**, 805–813.

Unguris, J., L. Bruch, E. Moog, and M. Webb: 1979, 'Xe adsorption on Ag(111): Experiment'. *Surface Science* **87**(2), 415 – 436.

von Issendorff, B. and R. E. Palmer: 1999, 'A new high transmission infinite range mass selector for cluster and nanoparticle beams'. *Review of Scientific Instruments* **70**(12), 4497–4501.

Wang, B., B. Yoon, M. König, Y. Fukamori, F. Esch, U. Heiz, and U. Landman: 2012, 'Size-Selected Monodisperse Nanoclusters on Supported Graphene: Bonding, Isomerism, and Mobility'. *Nano Letters* **12**(11), 5907–5912.

Wang, L.-S., X. Li, and H.-F. Zhang: 2000, 'Probing the electronic structure of iron clusters using photoelectron spectroscopy'. *Chemical Physics* **262**(1), 53 – 63.

Weiss, N., T. Cren, M. Epple, S. Rusponi, G. Baudot, S. Rohart, A. Tejeda, V. Repain, S. Rousset, P. Ohresser, F. Scheurer, P. Bencok, and H. Brune: 2005, 'Uniform Magnetic Properties for an Ultrahigh-Density Lattice of Noninteracting Co Nanostructures'. *Phys. Rev. Lett.* **95**, 157204.

Wortmann, B., K. Mende, S. Duffe, N. Grönhagen, B. von Issendorff, and H. Hövel: 2010, 'Ultraviolet photoelectron spectroscopy of supported mass selected silver clusters'. *physica status solidi (b)* **247**(5), 1116–1121.

Zimmerman, J. A., J. R. Eyler, S. B. H. Bach, and S. W. McElvany: 1991, 'Magic number carbon clusters: Ionization potentials and selective reactivity'. *The Journal of Chemical Physics* **94**(5), 3556–3562.

Acknowledgement

Ein großer Dank für die Hilfe bei der Erstellung dieser Arbeit geht an Herrn **Prof. Dr. Heinz Hövel** für die Vergabe des spannenden Themas in der Clusterphysik. Insbesondere danke ich für eine herausragende Betreuung während der vier Jahre am Lehrstuhl, die sich besonders dadurch auszeichnete, dass immer Zeit für Fragen aller Art war. Außerdem danke ich für die vielen interessanten und anregenden Gespräche mit und ohne physikalischem Kontext. Seine freundliche und entspannte Art gestaltete das Arbeiten am Lehrstuhl sehr angenehm.

Herrn **Prof. Dr. Metin Tolan** danke ich für die Möglichkeit meine Arbeit an seinem Lehrstuhl anfertigen zu dürfen.

Für die Übernahme der Zweitkorrektur danke ich Herrn **Prof. Dr. Dmitri Yakovlev**.

Prof. Dr. Frithjof Anders für die Übernahme des Prüfungsvorsitzes und **Dr. Gerald Schmidt** für Vertretung der wissenschaftlichen Mitarbeiter im Prüfungskomitee.

Für das zur Verfügung stellen des Fachwissens und der Materialien für die Präparation der Oxidproben danke ich **Prof. Dr. Conrad Becker**.

Prof. Dr. Bernd von Issendorff danke ich für die Beratung bezüglich der Clusterquelle und Interpretation von Photoelektronenspektren.

Ich danke **Dr. Natalie Swientek** für die Einführung in den Umgang mit der Messapparatur und für die unterhaltsame gemeinsam verbrachte Arbeitszeit.

Auch **Paul Salmen**, **Dominik Wolter**, **Matthias Bohlen** und **Raphael Floegel** danke ich für die schöne im Labor verbrachte Zeit und das gemeinsame Aufnehmen von Messdaten.

Für viele lustige und unterhaltsame Stunden in Kaffeepausen danke ich **Dominik Wolter**, **Paul Salmen**, **Stefanie Roese**, **Julian Schulze** und **Raphael Floegel**.

Manuela Linke, **Thorsten Witt**, **Georg Jülicher**, **Klaus Wiegers**, dem **Präparationslabor**, der **mechanischen** und der **Elektronik-Werkstatt** danke ich für die zahlreichen administrativen und technischen Hilfeleistungen.

Dem gesamten **Lehrstuhl EIa** danke ich für die tolle Atmosphäre während der Arbeit und auf Betriebsausflügen.

Ein besonderer Dank geht an meine Eltern **Anette** und **Joachim Schröder**, die mich immer unterstützt haben. Sie haben mir mein Studium ermöglicht sowie mein naturwissenschaftliches Interesse früh geweckt und gefördert.

Meinen Bruder **Stefan Schröder** und seiner Freundin **Inga Faller** danke ich für viele anregende Geschpräche und eine tolle Freundschaft.

Meiner Freundin **Miriam Sonnenschein** danke ich für den Halt und die Unterstützung, die sie mir gibt.

Meiner gesamten **Familie** und meinem **Freundeskreis** danke ich für die Möglichkeit in ihrer Gegenwart mal abschalten zu können.